NASA TECHNICAL NOTE

NASA TN D-4437

NASA TN D-4437

EFFECT OF TWO-DIMENSIONAL MULTIPLE SINE-WAVE PROTRUSIONS ON THE PRESSURE AND HEAT-TRANSFER DISTRIBUTIONS FOR A FLAT PLATE AT MACH 6

by Aubrey M. Cary, Jr., and E. Leon Morrisette

Langley Research Center

Langley Station, Hampton, Va.

NATIONAL AERONAUTICS AND SPACE ADMINISTRATION • WASHINGTON, D. C. • MARCH 1968

NASA TN D-4437

EFFECT OF TWO-DIMENSIONAL MULTIPLE SINE-WAVE PROTRUSIONS ON THE PRESSURE AND HEAT-TRANSFER DISTRIBUTIONS FOR A FLAT PLATE AT MACH 6

By Aubrey M. Cary, Jr., and E. Leon Morrisette

Langley Research Center
Langley Station, Hampton, Va.

NATIONAL AERONAUTICS AND SPACE ADMINISTRATION

For sale by the Clearinghouse for Federal Scientific and Technical Information
Springfield, Virginia 22151 – CFSTI price $3.00

EFFECT OF TWO-DIMENSIONAL MULTIPLE SINE-WAVE PROTRUSIONS ON THE PRESSURE AND HEAT-TRANSFER DISTRIBUTIONS FOR A FLAT PLATE AT MACH 6

By Aubrey M. Cary, Jr., and E. Leon Morrisette
Langley Research Center

SUMMARY

Surface pressure and heat transfer were measured and oil-flow patterns were observed on two-dimensional, shallow, multiple sine-wave protrusions embedded in a flat surface. The maximum laminar heating on multiple waves was found to correlate empirically with results from previous investigations. The maximum turbulent heating for a series of waves decreased rapidly from wave to wave. Tests with single waves and with the first wave of the multiple-wave model indicated that the maximum turbulent heating on single waves increased almost linearly with decreasing width-height ratio of the wave. The method used to predict the maximum turbulent heating gave fair results when there was no boundary-layer separation prior to the wave.

INTRODUCTION

In the development of hypersonic flight vehicles one of the design parameters of interest is the aerodynamic heating incurred on the vehicle surface. Methods for estimation of the heating on smooth surfaces are available, but practical surfaces may have irregularities and discontinuities.

Surface irregularities on a vehicle may be due to aerodynamic heating, pressure loading on the structure and skin, or to a particular choice of structural design. Numerous investigations have been conducted at supersonic speeds (refs. 1 to 4) and at hypersonic speeds (refs. 5 to 11) to determine the effect of particular types of protuberances on local surface pressure and heating. Effects of large, single, three-dimensional protuberances and of two- and three-dimensional protuberances in turbulent flow were presented in references 3 and 9 and in reference 1, respectively. The effects of one protuberance in the wake of another was also discussed in reference 1. Results of investigations of the effects of shallow two- and three-dimensional multiple protuberances were presented in references 7 to 10 for laminar flow, references 2 and 4 for turbulent flow, and references 5 and 6 for laminar and turbulent flow. Of particular interest are the results given

in reference 6 for which a semiempirical analysis for the peak values of heating for a two-dimensional wave in supersonic flow was developed.

Bertram (ref. 7) has presented results on the effect of single surface distortions on the local laminar heat transfer to blunt- and sharp-leading-edge flat wings and has indicated that the maximum heating obtained on the surface distortions could be correlated. The purpose of the present investigation is to determine the effects of a train of essentially two-dimensional sine-wave surface protrusions on the pressure and the predominantly turbulent heat transfer to flat plates with sharp and blunt leading edges. The use of a train of sine-wave protrusions is intended to simulate multiple surface protrusions, where one protrusion is in the wake of another. The bulk of the results obtained are for transitional or turbulent boundary-layer flow over the surface. Turbulent flow was obtained with both natural and roughness-induced transition. All the present results were obtained on an unswept plate in the Langley 20-inch Mach 6 tunnel. The wall-to-free-stream total temperature ratio was approximately 0.6 and the angle of attack and nose bluntness were varied to yield local Mach numbers from 2 to 6.8. Undistorted-flat-plate results corresponding to the multiple-surface-protrusion results are presented for comparison purposes.

SYMBOLS

C	linear viscosity coefficient, $\frac{\mu_w T_o}{\mu_o T_w}$
C_f	local skin-friction coefficient
C_F	average skin-friction coefficient based on local conditions
$C_{p,p}$	laminar plateau or turbulent first peak pressure coefficient
c_p	specific heat of air at constant pressure
c_w	specific heat of skin material
h	film coefficient of heat transfer, $\frac{\dot{q}}{T_{aw} - T_w}$
$\frac{\Delta h}{h_{fp}}$	heat-transfer parameter, $\frac{h_{max} - h_{fp}}{h_{fp}}$
H	maximum height of surface protuberance

K	roughness height, 0.198 cm
L	length of sharp-leading-edge model, 40.6 cm
M	Mach number
N_{St}	Stanton number, $\frac{\dot{q}}{\rho u c_p (T_{aw} - T_w)}$
p	static pressure
N_{Pr}	Prandtl number
$\dot{q}$	surface heat-transfer rate
r	recovery factor
R	Reynolds number
t	leading-edge thickness
T	temperature
T'	reference temperature
u	velocity
v	distance from virtual origin of boundary layer
W	width of surface protuberance
x	longitudinal distance along flat plate measured from leading edge or geometric stagnation point
x_d	distance to start of protuberance
α	angle of attack of instrumented surface
γ	ratio of specific heats for air

δ^*	displacement thickness of boundary layer
δ	boundary-layer thickness
λ	local wall thickness
θ	boundary-layer momentum thickness
μ	dynamic viscosity
ρ	density
τ	time
$\overline{\chi}_o$	viscous interaction parameter, $\frac{M_o^3\sqrt{C}}{\sqrt{R_{o,x}}}$

Subscripts:

aw	adiabatic wall
e	local conditions at outer edge of boundary layer
fp	flat plate
L	laminar
max	maximum
o	inviscid sharp-leading-edge value
t	stagnation
T	turbulent
v	based on distance from virtual origin
w	wall

x based on distance from leading edge or geometric stagnation point

∞ undisturbed free stream

APPARATUS AND TESTS

Wind Tunnel

The test program was conducted in the Langley 20-inch Mach 6 tunnel, which is of the blowdown type exhausting to the atmosphere through a movable second minimum with the aid of an annular ejector. The nozzle block is two dimensional and contoured. For this investigation the air was preheated to provide a stagnation temperature of approximately 517° K, while the stagnation pressure was varied from 7 to 35 atmospheres. A calibration of the test core (approximately 41 by 41 cm) indicates that the spanwise Mach number distribution is 6 ± 0.02 and the longitudinal variation through the test section is 6 ± 0.01. A more detailed description of the tunnel can be found in reference 12.

Models

The models used for this investigation had a wedge section with a total angle of 10°. One surface of the wedge was flat whereas a section of the other wedge surface consisted of a train of two-dimensional sine waves. A section of flat surface preceded and followed the sine-wave section. A sharp-leading-edge ($t \approx 0.0076$ cm) wedge wing and a blunt-leading-edge ($t \approx 1.9$ cm) wedge wing were constructed and instrumented for measuring surface static pressures, and an externally identical set was constructed and instrumented for measuring surface heat transfer. A drawing of the sharp- and blunt-leading-edge models superimposed, with the pertinent dimensions and instrumentation orientation, is given in figure 1. The chordwise locations of the instrumentation are listed in table I and are shown for a typical wave in figure 1. The two different sets of end plates used for all tests in this investigation, one with the sharp-leading-edge model and the other with the blunt-leading-edge model, are shown as outlines in the figure. The end plates were designed to enclose the leading-edge shock at all angles of attack. The wave train consisted of sine waves with five peaks, each wave having a half-wavelength of 1.9 cm and an amplitude of 0.25 cm. The size and number of the waves were arbitrarily chosen to represent multiple surface protuberances on a plane surface.

The pressure models were constructed of stainless steel, and the instrumented surface was 0.152 cm thick. The pressure orifices had an inside diameter of 0.254 cm. The underframes of the heat-transfer models were constructed of steel, and the instrumented surface, nominally 0.076-cm-thick inconel, was insulated from the underframe with fiber

glass at support points. Thirty-gage chromel-alumel thermocouples were spotwelded to the undersurface of the multiple-wave heat-transfer models at the locations indicated.

The heat-transfer models were utilized with the surface smooth and with roughness elements, intended to trip the boundary layer, 5.08 cm back from the leading edge for the sharp-leading-edge model. The roughness elements were 0.198-cm-diameter spheres spotwelded to the surface 0.79 cm apart across the span of each side of the wedge. The size and location of the surface roughness elements were selected following the results of reference 13. The value of K/δ for the present investigation varied from 1.0 at $\alpha = -5^{\circ}$ to 5.9 at $\alpha = 15^{\circ}$, where δ was calculated by using the laminar T' equation of reference 14.

The sharp-leading-edge heat-transfer model was modified by replacing the flat surface of the wedge by other inconel plates which had a single half-wavelength sinusoidal protuberance near the rear. A sketch of this arrangement is shown in figure 2. The amplitude of the single protuberances was kept constant at approximately 0.43 cm, whereas the half-wavelengths were 2.54 cm, 5.08 cm, and 10.16 cm. The corresponding beginning of the sine wave was 26.4 cm, 26 cm, and 24.7 cm back from the leading edge. Thirty-gage iron-constantan thermocouples were spotwelded to the undersurface of the 0.076-cm-thick inconel inserts at the locations given in table II. The roughness size and location were the same as for the sharp-leading-edge multiple-wave model. The plate leading edge for the single-wave tests was approximately 0.00254 cm thick.

Test Methods

Variation in local Mach number was accomplished by mounting the models at angle of attack in the test section of the Langley 20-inch Mach 6 tunnel. The local Mach number M_e was calculated by utilizing the measured surface pressure distribution and oblique shock relations for the sharp-leading-edge plate and the measured surface pressures with the assumption for the blunt-leading-edge plate that the plate boundary layer is immersed in the high-entropy layer associated with the near-normal portion of the leading-edge shock. The calculated local Mach number for each of the plates at angle of attack in the Mach 6 stream is given in the table.

Leading edge	α, deg	M_e
Sharp	-5	6.8
	0	6.0
	5	5.3
	10	4.6
	15	4.0
Blunt	-5	2.6 to 3.2
	0	2.4 to 2.9
	5	2.2 to 2.6
	10	2.0 to 2.3
	15	1.8 to 2.0

Oil flow.- Surface flow patterns were obtained by using the oil-flow technique. A mixture of oil and lampblack was applied in a random dot pattern to a model before a test. The model, in a shielded position, was rapidly exposed (0.25-second injection time) to the established tunnel test flow, allowed to remain in the flow approximately 3 seconds, and then rapidly extracted from the flow. The direction and extent of movement of the oil droplets then allowed a qualitative analysis of the surface flow over the models.

Pressure.- The static pressures were measured by connecting the orifices to pressure-switching devices which in turn connected the orifice in sequence to electrical pressure transducers. The pressure from each orifice was sensed by a 0 to 7×10^3, a 0 to 3.5×10^4, and a 0 to 1×10^5 N/m^2 transducer. This arrangement allowed the most accurate results since the static pressure could be obtained from the transducer with the range nearest full-scale reading. The accuracy of all transducer readings was 0.25 percent of full-scale reading.

Heat transfer.- Aerodynamic heating was determined by the transient calorimetry technique by which the rate of heat storage in the model skin was measured. The models, initially at room temperature, were exposed to the airstream from a shielded position. Injection was accomplished in approximately 0.25 second.

Test Conditions

The conditions for the tests with the various models used in this investigation are as follows:

Model	Leading edge	Type of data	Boundary-layer trip	α, deg	R_∞/cm	T_w/T_t
Multiple wave	Sharp and blunt	Pressure	No	-5, 0, 5, 10, 15	0.21×10^6	0.89
Multiple wave	Sharp and blunt	Heat transfer	No	-5, 0, 5, 10, 15	0.26×10^6 .165 .087	0.6
Multiple wave	Sharp	Heat transfer	Yes	0, 5, 10, 15	0.26×10^6 .165 .087	0.6
Single wave	Sharp	Heat transfer	Yes	0, 15	0.27×10^6 .14 .063	0.6
Multiple wave	Blunt	Oil flow	No	-5, 0, 5, 10, 15	0.26×10^6 .165 .087	0.6
Multiple wave	Sharp	Oil flow	Yes	0, 5, 15	0.26×10^6 .165 .087	0.6
Single wave	Sharp	Oil flow	Yes	0, 15	0.27×10^6 .14 .063	0.6

Oil-flow patterns were obtained on the heat-transfer models. Although some oil-flow patterns were obtained by using the sharp-leading-edge multiple-wave model with roughness, damage to the model surface made presentation of oil-flow patterns for the sharp-leading-edge model without roughness impractical.

DATA REDUCTION

Pressure

The electrical outputs from the pressure transducers were recorded on a high-speed digital readout recorder. Through the use of calibration data for each transducer the electrical outputs were converted to pressure readings on a card programed computer.

Heat Transfer

The electrical outputs from the thermocouples were recorded on a high-speed digital readout recorder. The signal from each thermocouple was sampled 20 times each second, converted to a binary digital system, and recorded on magnetic tape. Beginning when the model was positioned at the center line of the test section, 1 second of the temperature-time data was fitted to a second-degree polynomial by the method of least squares. The time derivative of temperature used to calculate the heating coefficients was computed at the first point of the curve fit (the derivative was constant for approximately the first five points).

The model wall temperature at the start of the tests was approximately 306° K. Because of the quick insertion into the test flow, the models were considered to have been subjected to a step function in aerodynamic convective heat input. In the absence of radiative and conductive heat losses, the local surface heating rate for the models was expressed as

$$\dot{q} = c_w \rho_w \lambda \frac{dT_w}{d\tau}$$

where $c_w = 436 + 0.140\left(\frac{9T_w}{5} - 460\right)$ J/kg°-C, $\rho_w = 8540$ kg/m^3, and T_w is in °K. For conversion to local heat-transfer coefficient the adiabatic wall or recovery temperature was taken to be

$$T_{aw} = T_e\left(1 + rM_e^2 \frac{\gamma - 1}{2}\right)$$

The recovery factor r was calculated by assuming that for heat transfer in laminar flow

$$r = \sqrt{N_{Pr}}$$

and for heat transfer in turbulent flow

$$r = \sqrt[3]{N_{Pr}}$$

where the Prandtl number (ref. 15) corresponded to Monaghan's laminar or turbulent T' temperature (ref. 14). The Stanton number was based on free-stream conditions ahead of the model.

Radiative heat losses were negligible in the temperature range of this investigation. In the vicinity of the surface protuberances the maximum surface temperature rise was generally between 20° and 40°. The temperature rise of the flat surfaces was generally less than 15°. No conduction corrections were applied to the data of this report, since for the most critical case reported the calculated heat conduction determined from the measured wall temperatures and the three-point finite-difference method of reference 16 amounted to less than 5 percent of the convective heat input. Conduction errors for most of the data were less than 3 percent.

RESULTS AND DISCUSSION

Transition

For the proper orientation of the reader to the flow conditions of this investigation, the locations of boundary-layer transition determined from the surface heat-transfer data presented later in this report for the sharp- and blunt-leading-edge flat plates are defined in figure 3. Results are presented for the models with and without the boundary-layer trip and through the angle-of-attack and Reynolds number ranges of this investigation. The boundary-layer trip for the blunt plate was a small step ($H \approx 0.0076$ cm) which inadvertently occurred near the nose—flat-plate junction for a series of tests. The results of figure 3 may be used to augment the oil-flow and heat-transfer tests.

Surface Oil Flow

No roughness.- As previously mentioned, the surface of the sharp-leading-edge multiple-wave model was damaged before oil-flow tests were initiated. Representative surface oil-flow patterns for the models with no roughness are presented for the blunt leading edge only. In general, comments concerning the blunt-leading-edge model oil-flow patterns may be interpreted as representative as those for the sharp-leading-edge model, since tests with the damaged model and other tests at Mach 6.8 indicate the similarity of the oil-flow patterns.

Examples of the surface oil-flow patterns on the blunt-leading-edge multiple-wave model are shown in figure 4. Areas of surface flow where the boundary layer is attached

or separated can presumably be observed from surface oil-flow patterns. Reference 17 indicates that for an adverse pressure gradient acting on a turbulent boundary layer, surface oil may accumulate at a position other than a separation location due to wind forces acting downstream and buoyancy forces acting upstream. Therefore, all separations at the first wave were verified where possible by the surface pressure measurements presented later in this report. Oil-flow studies indicate that the surface shear develops normally until the adverse pressure gradient due to the first wave causes the boundary layer for laminar and transitional flow to separate from the plate surface (fig. 4(a)). The extent of boundary-layer separation preceding the first wave is a function of the local flow conditions. Generally, for the tests without roughness the separation length decreases with increasing angle of attack at a constant free-stream Reynolds number and decreases with increasing Reynolds number at a constant angle of attack. This effect is taken to indicate a trend from laminar to turbulent flow. After the initial separation, the boundary layer reattaches to the front portion of the first sine-wave protrusion, remains attached over the top portion, and then reseparates as the boundary-layer flow expands over the rear of the first sine wave. The separated boundary layer then traverses the sine-wave cavity between the first and second waves approximately level with the flat surface preceding the waves and reattaches to the face of the second wave. The surface flow patterns are similar as the boundary layer traverses the remaining sine-wave protrusions. As the boundary-layer flow expands over the rear of the last wave, there is a region of separated flow before reattachment to the flat surface. For several tests where the boundary layer was essentially turbulent at the first wave there was no appreciable extent of separation preceding the wave, but the patterns on the remaining waves were essentially as previously described (fig. 4(c)).

An interesting pattern observed in the oil-flow studies is seemingly three-dimensional fluid motion of paired vortices in the separated regions of the sine-wave cavities. These patterns are shown in the blown-up portion of figure 4(b); they appear to be more prevalent near the end plates and damp out in some cases toward the center of the plate. In an attempt to determine the origin of the vortices, several oil-flow patterns were obtained on the blunt-leading-edge plate with one end plate missing. The results of one of the tests are shown in figure 4(d). In the separated regions near the side of the model without the end plate, there is observed a definite outflow of the oil as the flow expands from the pressure in the separated regions to the lower free-stream pressure. The vortices do not appear near the side of the model without the end plate. In the separated regions near the side of the model with the end plate the flow patterns remain essentially unchanged. The vortex-like motion in the separated regions of the sine-wave cavities may result from end-plate effects which extend across the plate in the separated region between waves. It is also possible that the occurrence of the

vortices in the separated regions is a transition-turbulence phenomenon, since the vortices occurred only when the plate boundary layer was transitional or turbulent.

Roughness.- Examples of the surface oil-flow patterns obtained by using the sharp-leading-edge model with surface roughness are shown in figure 5. The oil streaks behind the roughness elements may indicate discrete spanwise regions of higher and lower shear as a result of the roughness elements or may be the result of spanwise movement of the oil without a necessarily significant change in the shear. Heat-transfer tests under the same conditions indicate that there is no noticeable spanwise effect on the heating distributions as a result of the roughness elements.

For all the tests with roughness, the indicated separation region preceding the first wave was small (in contrast to the tests with no roughness). This small region of indicated separation is taken to be characteristic of the turbulent boundary layer in the vicinity of the first wave. The flow patterns over the remaining waves are essentially as previously described.

Surface Pressures Without Roughness

The pressure distributions for the multiple-wave plates and the corresponding smooth plates are presented in figure 6 for the sharp-leading-edge plate and in figure 7 for the blunt-leading-edge plate. A typical pressure distribution (e.g., fig. 6(b)) shows an increase in pressure on or just ahead of the first wave with the pressure reaching a maximum value near reattachment for separated flow and near the start of the wave for attached flow. After traversing the first wave the boundary layer separates from the rear of the wave, and the surface pressure reaches a value near or below the smooth-plate level. This pattern of rising and falling pressures is repeated on succeeding waves with the maximum pressure occurring near reattachment and the minimum pressure occurring in the valleys.

Smooth-plate distributions.- Figures 8(a) and 8(b) give the smooth-plate pressure distributions for the sharp- and blunt-leading-edge models, respectively. The data obtained by using the sharp-leading-edge model are compared with predictions for $\alpha = -5^{\circ}$, 5°, and 15° of the weak-interaction equation of reference 18. This equation in the present nomenclature is as follows:

$$\frac{p}{p_o} = 1 + \frac{\frac{\gamma G}{2}\bar{\chi}_o}{\sqrt{1 + \frac{\gamma G}{2}\bar{\chi}_o}}\left[1 + \frac{\frac{\gamma G}{2}\bar{\chi}_o}{2\left(1 + \frac{\gamma G}{2}\bar{\chi}_o\right)}\right] + \frac{\gamma + 1}{4\gamma}\frac{\left(\frac{\gamma G}{2}\bar{\chi}_o\right)^2}{1 + \frac{\gamma G}{2}\bar{\chi}_o}\left[1 + \frac{\frac{\gamma G}{2}\bar{\chi}_o}{2\left(1 + \frac{\gamma G}{2}\bar{\chi}_o\right)}\right]^2 \qquad (1)$$

where $G = 1.72 \frac{\gamma - 1}{2}\left(\frac{T_w}{T_{aw}} + 0.352\right)$ for a Prandtl number of 0.725. The wall temperature was assumed to correspond to that for a recovery factor of 0.89 which agreed well with the temperatures measured during the pressure tests. The experimental data are slightly higher than the predictions from equation (1) at $\alpha = -5^o$, and agreement with theory improves with increasing angle of attack.

The blunt-leading-edge data are compared with the blast-wave correlation of reference 19; agreement is good at all angles of attack.

Maximum pressures on multiple waves.- In figures 6 and 7 it is indicated that the maximum pressures on the multiple waves decrease with increasing distance from the leading edge for both laminar (fig. 6(a)) and turbulent (fig. 6(e)) flow. However, for transitional flow, the maximum pressures increase with distance from the leading edge before they decrease (e.g., fig. 6(c)).

Figure 9 presents the first plateau and maximum pressures for the first wave nondimensionalized by the smooth-plate value at the same location for both plates through the angle-of-attack range. In some cases the plateau pressure was not well defined, and an average of the pressures in the indicated plateau region was used as the plateau pressure (e.g., figs. 6(d) and 7(d)). Given in figure 9 are the separation parameters calculated by using the semiempirical relations of reference 20 for the laminar plateau pressure and turbulent first peak pressure. The equation used to obtain the laminar plateau pressure coefficient is

$$C_{p,p} = \frac{\left(2.61 M_e^{-1/4}\right)(C_f)^{1/2}}{\left(M_e^2 - 1\right)^{1/4}} \tag{2}$$

The turbulent first peak pressure coefficient is given by the following equations:

$$C_{p,p} = \frac{3.2}{8 + (M_e - 1)^2} \tag{3}$$

for $M_e = 1$ to 4 and

$$C_{p,p} = 0.13 - \frac{1.5}{M_e^2} + \frac{9.1}{M_e^3} \tag{4}$$

for $M_e = 3.5$ to 7.

The trend of laminar plateau pressures with Mach number is in fair agreement with that of predictions from equation (2) but is slightly higher. The maximum pressures measured on the waves are only slightly above the plateau values for laminar separation (10 to 15 percent). The maximum first wave pressures for turbulent flow are consistently higher than the calculated turbulent first peak pressures. This underprediction is

expected since the turbulent first peak pressure is a separation phenomenon which occurs before the final pressure is reached (in this case p_{max}) and does not occur for nonseparated flow. Where the boundary layer was essentially turbulent at the first wave ($\alpha = 10^{o}$ and 15^{o} for the sharp-leading-edge plate and $\alpha = 15^{o}$ for the blunt-leading-edge plate), oil-flow studies indicate no noticeable separation. The maximum pressures where the flow is transitional fall between those for laminar and turbulent flow as would be expected.

Surface Heating on Multiple-Wave Models

The aerodynamic heat-transfer distributions obtained on the multiple-wave models at a free-stream Mach number of 6 are shown in figure 10 for the sharp-leading-edge model and in figure 11 for the blunt-leading-edge model. Data with and without surface roughness are presented for the sharp-leading-edge model, whereas data obtained without surface roughness are presented for the blunt-leading-edge model. In general, the correlation of the major lines of spanwise thermocouples for both the sharp- and blunt-leading-edge models with and without surface roughness was good. Occasionally the beginning of boundary-layer transition on the plate surface without roughness would vary slightly over the span of instrumentation; this in turn yielded a noticeable variation in the heating rates (fig. 10(d)). When a variation occurred, symbols along the same line of instrumentation were joined by a smooth curve. Additional spanwise thermocouples were also installed at various chordwise locations on the model surfaces (fig. 1) to indicate the two dimensionality of the surface flow. The heating values from these thermocouples are shown to be typical in figure 10(a) and are distinguished by a tick mark on each side of the symbol. In general, the results from the spanwise instrumentation show small effects when the plate boundary layer is laminar or turbulent. When the boundary layer is transitional, substantial variations in spanwise heating occasionally occur. From the heating distributions it is inferred that transition does not always occur at the same chordwise location for each line of instrumentation.

No roughness.- Variations of the smooth-plate heating with Reynolds number and Mach number for the laminar or turbulent boundary layer are as expected and may be predicted by theory (see section entitled "Analysis of Surface Heating").

The heating distributions for the sharp- or blunt-leading-edge multiple-wave plates are essentially the same as those for the comparable smooth plates on the forward portion of the plate, but a radical variation from the smooth-plate heating occurs as the waves begin to influence the surface flow. When the boundary layer is laminar, separation occurs ahead of the first wave, and as characteristic of laminar separation, the surface heating drops significantly below the corresponding smooth-flat-plate heating (e.g., fig. 10(a)). As the flow reattaches to the face of the first wave the heating rises well above the flat-plate heating. Oil-flow studies indicate that the boundary layer remains

attached over the top portion, separates from the rear of the first wave as the flow expands into the cavity, and then reattaches to the surface of the second wave. Before reattachment to the second wave the heating drops below the flat-plate level. The flow mechanics are very similar for the remaining four waves, yielding a series of maximum heating values on the wave peaks and a series of minimum heating values in the wave cavities. As the flow expands over the last wave, the surface heating drops below the flat-plate value as the boundary layer separates and rises above flat-plate heating as the boundary layer reattaches to the flat surface. The maximum heat transfer to the protuberances was near reattachment on the face of each wave. The minimum heating occurs a short distance after the boundary layer separates from the rear of the protuberance. When transition occurs before boundary-layer separation preceding the first sine wave, there is little or no drop below smooth-plate heating in the initial separated region (square symbols in fig. 10(b)). The heating trends for the following waves remain essentially as previously described.

For the lower local Reynolds numbers the maximum heating on the waves decreases with increasing Reynolds number (fig. 10(a), $R_\infty/cm = 0.083 \times 10^6$). When the local Reynolds number is increased, the maximum heating begins to increase (fig. 10(a), $R_\infty/cm = 0.26 \times 10^6$) until beyond a certain Reynolds number the maximum heating begins to decrease with increasing Reynolds number in a manner similar to that for the lower local Reynolds numbers (circular symbols in fig. 10(d), $R_\infty/cm = 0.165 \times 10^6$). It is reasonable to relate the described variation of the maximum heating with Reynolds number to laminar, transitional, and turbulent flow for the waves. Therefore, when transition occurs over the waves, the boundary layer is considered turbulent when after an increase in maximum heating values the maximum heating for successive waves is decreasing with increasing Reynolds number.

Comparing the heating distributions for the sharp-leading-edge flat plate and the sharp-leading-edge multiple-wave plate at the same flow conditions (fig. 10) indicates that, in general, boundary-layer transition begins and ends at approximately the same location. Blunting the leading edge of the model markedly delayed the onset of boundary-layer transition for the smooth plate (cf. figs. 10(c) and 11(c)). For most of the data the heating trends for the wave surface on the blunt-leading-edge plate indicate that the series of waves promote transition on the distortion surface well before transition occurs on the flat surface.

Roughness.- The heating distributions obtained for the fully developed turbulent boundary layer by using surface roughness (figs. 10(b) to (e)) were similar to those obtained without roughness, the obvious differences being related to the location of transition. The maximum heating steadily decreases from the first peak to the fifth peak when the plate boundary layer is fully turbulent approaching the first peak.

Analysis of Surface Heating

Flat plate.- Since flat-plate heating data are used to normalize corresponding maximum heating on the waves, comparisons of the flat-plate data with appropriate theoretical predictions are presented in figures 12 and 13.

The laminar data for the sharp-leading-edge flat plate are compared in figure 12 with results from the method presented in reference 20 which utilizes the T' equation of reference 14, the computations of Van Driest presented in reference 21, and predictions from the "$\rho_r \mu_r$" method presented in reference 22. The three methods yield approximately coincident predictions for the conditions of this investigation and underestimate the level of the data by approximately 20 percent. The laminar data for the blunt-leading-edge flat plate (fig. 12) are compared with predictions from the T' method applied "locally" to account for variable local flow conditions and predictions from the method of reference 23. The predictions from the T' method approximate the level and trend of the data especially at the higher angles of attack where the pressure gradient is less severe, whereas the predictions from reference 23 yield results which are substantially below the experimental data at all angles of attack.

Experimental results for turbulent heating on the sharp- and blunt-leading-edge flat plates are shown in figure 13. The data are presented as the variation of free-stream Stanton number with free-stream Reynolds number based on the distance from the hypothetical "virtual origin" of turbulent boundary layer. The virtual origin for the data for both the sharp and blunt plates without surface roughness was taken to be at the end of transition (assumed to be the location of the peak flat-plate heating for each respective test). The virtual origin for the plates with surface roughness was assumed to be the roughness location or the location of peak heating if the peak occurred behind the roughness location. The validity of these assumptions is discussed in references 13 and 24. Most of the turbulent data for the blunt-leading-edge model were obtained by tripping the boundary layer with a small step near the shoulder of the leading edge.

The reference temperature method was used to predict the local skin friction for the blunt- and sharp-leading-edge flat plates. The turbulent reference temperature equation suggested by Monaghan (ref. 14) along with the Kármán-Schoenherr equation for local turbulent incompressible skin friction (ref. 25) and local flow conditions as previously defined were used to predict the turbulent skin friction. Equations and procedures for this method can be found in reference 20. Colburn's form of Reynolds analogy (eq. (A11) of ref. 20) factor based on the turbulent T' reference temperature was used to convert from skin-friction coefficients to heat-transfer coefficients. There is good agreement between experimental data and T' predictions for the sharp-leading-edge plate at all angles of attack. The blunt-leading-edge plate heat-transfer results are overpredicted by the T' method at all angles of attack.

The Spalding-Chi predictions for turbulent skin friction (ref. 26) using the Kármán form of Reynolds analogy (ref. 24) are also presented in figure 13. At all angles of attack the modified Spalding-Chi predictions are slightly lower than the data for the sharp-leading-edge plate but are in relatively good agreement with the data for the blunt-leading-edge model.

Maximum laminar heating on multiple waves.- Because of the absence of a rigorous analytical approach for predicting the laminar peak heating on a surface protuberance, an approach similar to that of reference 5 was used to correlate the peak heating values in laminar flow. As in reference 5 the laminar-boundary-layer displacement thickness in lieu of the boundary-layer thickness was used as the correlating parameter because of the relative difficulty in defining the boundary-layer thickness. Laminar values of the displacement thickness were calculated by using the method recommended by Monaghan in reference 14 and local flow conditions as previously defined. The assumption was made that δ_L^* was the same at a particular peak location as the corresponding flat plate δ_L^*.

The correlating parameter used was $\frac{M_e}{\delta_L^*/H}$ where M_e is the local Mach number calculated as previously described and δ_L^* is nondimensionalized by use of the maximum perturbation height H. The coefficient h_{fp} was determined from measured laminar flat-plate heat-transfer data taken at comparable locations and flow conditions as the corresponding peak heating value. Only the laminar peak heating data obtained at $\alpha = -5^o$ and 0^o for the sharp plate and $\alpha = -5^o$ for the blunt plate were used in this comparison. The heating data for the three successive sine-wave protuberances plotted in figure 14 correlate with the empirical prediction presented in reference 5 as

$$\frac{h_{max}}{h_{fp}} - 1 = \frac{1}{36}\left(\frac{M_e}{\delta_L^*/H}\right)^{1.9} \tag{5}$$

Reference 6 presents a method known as shallow-wave theory to predict the value of laminar peak heating for a single perturbation in attached supersonic flow. Shallow-wave theory indicates that the laminar peak heating should be a function of δ_L^* and M_e. The results obtained from shallow-wave theory for the particular conditions indicated are shown in figure 14 for comparison. Predictions from shallow-wave theory do not compare favorably with the experimental data. Since the derivation of the shallow-wave theory requires that there be no local boundary-layer separation in the vicinity of the surface protuberance, it is not surprising that agreement between the experimental data and shallow-wave predictions is poor.

Maximum turbulent heating on multiple waves.- Maximum turbulent heating on the multiple waves was obtained under two conditions, natural transition and forced or

roughness-induced transition. It is of interest to note whether the process of transition of a boundary layer while separating and reattaching along a wavy surface yields a turbulent boundary layer that is equivalent to one that has become turbulent on a flat, zero-pressure-gradient surface and then traverses the wavy surface. One indication of the equivalency of the two types of turbulent boundary layers would be a comparison of the maximum heating values for the multiple waves. This comparison is made in figure 15, where the turbulent maximum heating values for these tests and tests at $M_\infty = 7.95$ reported in reference 5 are plotted as the flat-plate correlation coordinates $N_{St,e,max}$ and $\left(\log_{10} R_{e,v}\right)^{2.58}$. The "virtual origin" for the multiple-wave results with roughness was taken to be the roughness location or the location of peak heating if the end of transition did not occur at the roughness location.

When boundary-layer transition occurs over the waves, the values of maximum turbulent heating obtained seem to correlate along a line having a slope ≈ -1. The minus-one-slope correlation holds for no-roughness sharp- and blunt-leading-edge data and for roughness sharp-leading-edge data where the end of transition occurred over the waves. At a local Reynolds number of approximately 10^6, $\left(\log_{10} R_{e,v}\right)^{2.58} \approx 100$, the slope of the no-roughness data increases sharply in a negative sense. Now, where the boundary layer was fully turbulent before the first wave the data seem to correlate along a line having a slope ≈ -2. Beyond a local Reynolds number of approximately 10^6, $\left(\log_{10} R_{e,v}\right)^{2.58} \approx 100$, turbulent data obtained under all conditions included in figure 12 correlate along the line having a slope ≈ -2. The results of figure 15 clearly indicate that for the assumptions utilized, the maximum heating values obtained with a boundary layer which is turbulent prior to a train of surface protuberances are equivalent to the heating values obtained when boundary-layer transition occurs over the protuberances only beyond a certain minimum turbulent Reynolds number. The choice of the virtual origin as the peak heating location at transition is indicated by comparison of various theories with flat-plate heating and skin-friction data. If the peak heating location is chosen to be the virtual origin for the turbulent boundary layer on a flat plate, experimental heat-transfer and skin-friction results indicate that data representative of a fully turbulent boundary layer are obtained only for an approximate value of local Reynolds number based on the distance from the virtual origin greater than 10^6 (e.g., see ref. 24). The results obtained with the flat plate would imply that the maximum heating data obtained with the multiple-wave plate for $R_{e,v} < 10^6$ would be indicative not of a fully turbulent boundary layer but of a transitional boundary layer.

Figure 16 presents the effect of Reynolds number on the maximum turbulent heating obtained on the train of waves for the sharp-leading-edge multiple-wave plate on which the boundary layer was tripped. For all the data presented in figure 16, the end of transition occurred before there was any effect of the surface protuberances on the boundary

layer. The plot coordinates of figure 16 were selected because the first peak maximum heating values appear to correlate as $\frac{1}{M_e}\frac{\Delta h}{h_{fp}}$ and $R_{e,v}$. Maximum heating values for succeeding waves are shown connected by dashed lines and in contrast to the laminar results fail to exhibit the same correlation as the first peaks. The effect of local unit Reynolds number on the maximum turbulent heating for the first peaks where only small separated regions appear prior to the peaks is similar to the Reynolds number effect on smooth plate turbulent heating. The turbulent maximum heating for a series of peaks succeeding a first peak decreases almost linearly with increasing Reynolds number.

For each Mach number and unit Reynolds number for which the end of transition occurred before the first wave, the maximum values of turbulent heating over the train of waves occur at the first peak, and the highest value of turbulent heating for each succeeding peak is significantly less than that for the preceding peak. Savage-Jaeck theory as presented in reference 6 and further explained in reference 5 is presented in figure 16 for comparison with the experimental data. In applying the Savage-Jaeck theory it is assumed that each wave is separate with no flow separation and that the local conditions are unaffected by previous waves. The calculation procedure for Savage-Jaeck theory requires the definition of a turbulent-boundary-layer displacement thickness δ_T^*. The following procedure was used to calculate δ_T^*:

(1) Calculate the laminar-boundary-layer momentum thickness θ_L at the assumed location of the virtual origin by using previously outlined methods.

(2) Assume that θ_L is the same as the turbulent-boundary-layer momentum thickness θ_T at the virtual origin.

(3) Calculate the new "virtual origin" for δ_T^* by using

$$\theta_T = \frac{vC_F}{2} \tag{6}$$

where C_F is given by Monaghan's turbulent T' method as presented in reference 14. With the new virtual origin, δ_T^* may be calculated for the turbulent portion of the boundary layer from the following equation:

$$\delta_T^* = \frac{vC_F(\delta^*/\theta)}{2} \tag{7}$$

where the boundary-layer form factor δ^*/θ was obtained from reference 27 with the exponent in the power law for velocity taken to be 1/9 (ref 28). The foregoing method permits the calculation of δ_T^* by assuming that the test surface is a flat plate. It was further assumed that δ_T^* at the location of the maximum turbulent heating for a particular wave was that of an equivalent flat plate. Savage-Jaeck theory under the included

assumptions would predict correlation of the turbulent maximum heating values for all waves at a given Mach number. The flow conditions for the first peak experimental data more closely adhere to the assumptions of the theory, and therefore these data would be more amenable for comparison with the theory. Savage-Jaeck predictions do not compare favorably with the data presented in figure 16.

Maximum turbulent heating on single waves.- Very little information concerning the effect of a variation of the geometric amplitude-to-wavelength ratio on the surface heating for the sine-wave protuberances is available from the previously presented multiple-wave results. Therefore, supplementary tests of single two-dimensional sine-wave protrusions on the sharp-leading-edge model with end plates were made in turbulent flow.

With this model surface oil-flow patterns and heating distributions were obtained at $\alpha = 0^{\circ}$ and 15° for surfaces with single waves having $W/H = 5.9$, 12.5, and 23.5. For each value of W/H, surface heating data were obtained for $M_{\infty} = 6.0$ and free-stream unit Reynolds numbers of approximately 0.27×10^6, 0.14×10^6, and 0.06×10^6 per cm. Flat-plate surface heating distributions for the same conditions used in the single-protuberance heating tests were obtained. The surface roughness size and spacing were the same as those used for the multiple-wave tests. The spherical roughness caused the end of transition to be in the vicinity of the roughness location for all test conditions except $\alpha = 0^{\circ}$ and $R_{\infty}/cm = 0.063 \times 10^6$. For these conditions obvious oil streaks on the protrusion were seen and corresponded one-to-one with the roughness spheres across the span of the plate.

A typical example of the heating distribution over the single waves is presented in figure 17 as the variation of $N_{St,\infty}$ with x at $\alpha = 0^{\circ}$ and $R_{\infty}/cm = 0.138 \times 10^6$. The turbulent flat-plate heating was generally predictable by using the modified Spalding-Chi method with the "virtual origin" again taken to be the location of peak heating at transition.

For the particular surface heating results shown in figure 17 oil patterns indicated that the flow was attached over the 10.16-cm-wide wave, there was a small region of separated flow after the 5.08-cm-wide wave, and there was a large separated region in front of and behind the 2.54-cm-wide wave. The turning angle necessary for turbulent separation for the waves was consistent with results previously presented for wedges and concave corners (e.g., ref 29). As the flow compressed at the front of the wave for either attached or separated flow, there was a sharp rise above the flat-plate heating. A maximum value of surface heating was obtained either directly after the start of the wave or with separation preceding the wave a short distance after reattachment to the wave surface. As the flow expanded over the top of the wave, the heating decreased sharply and reached a value well below flat-plate heating very near the wave—flat-surface intersection. As the flow recompressed on the flat surface for the attached boundary

layer and near reattachment for the separated boundary layer, there was a rise in surface heating quickly approaching the flat-plate heating. The heat transfer in the turbulent separated region in front of the 2.54-cm-wide wave decreased slightly below the flat-plate level (see fig. 17 as typical). Although previous investigations (e.g., ref. 20) have shown that an increase in heating in the separated region for a turbulent wedge-type separation is to be expected, the reversal of the pressure gradient at reattachment for the wave separation may have influenced the heating level. (The present results are based on limited evidence and a more extensive investigation would be necessary for clarification.)

Boundary-layer separation in front of a wave has only a minor effect on the surface heating in the separated region, but the separation phenomenon seems to have a significant effect on the maximum surface heating obtained on a wave. Figure 18 indicates the effect of width-height ratio and boundary-layer separation on the maximum heating obtained on a wave. The maximum heating on a single wave appears to increase almost linearly with decreasing W/H. The Savage theory adapted to turbulent flow by Jaeck gives a fair estimate of the maximum heating except where the boundary layer is separated prior to the wave. Where there is more extensive separation, the 2.54-cm-wide wave, Savage-Jaeck theory seriously underestimates the maximum heating. The photographs in figure 18 show the surface oil-flow patterns obtained for the protuberance surfaces indicated. The data with the dashed ticks are those for which no oil-flow patterns were obtained but for which separation was inferred from the surface heating distribution and oil-flow patterns obtained for other waves.

Included in figure 18 are the first peak maximum turbulent heating data obtained by using the sharp-leading-edge, multiple-wave model with surface roughness (W/H = 7.5). For these data the boundary layer was fully turbulent in front of the wave. The maximum heating for the first peak of the multiple-wave plate compares favorably with the single-wave results. The comparison should be good since the values of δ_T^*/H at the first peak for the multiple-wave tests are approximately the same as those for the single-wave tests.

CONCLUSIONS

An investigation of the effects on surface pressure and heat transfer of two-dimensional, shallow, multiple protuberances embedded in a flat surface has been conducted at Mach 6. Tests were conducted with sharp-leading-edge wedge wings with and without a boundary-layer trip and blunt wedge wings without a boundary-layer trip over a free-stream Reynolds number range based on model length of approximately 3.2×10^6 to 11.4×10^6 and a wall-to-free-stream total temperature ratio of approximately 0.6. Supplementary heat-transfer tests were also conducted with the sharp-leading-edge wing

with a boundary-layer trip and single protuberances. An analysis of the information obtained in this investigation yielded the following conclusions:

1. The maximum laminar heating on multiple waves was found to correlate empirically with results from previous investigations. Succeeding waves in the train of waves were amenable to an analysis which considers each wave in the train as a single wave and independent of the other waves on the plate.

2. For a given local Mach number, the effect of local unit Reynolds number on the maximum turbulent heating for the first wave, or single waves, was similar to the Reynolds number effect on smooth flat-plate turbulent heating. The turbulent maximum heating for a series of waves succeeding a particular first wave decreased almost linearly with increasing local Reynolds number.

3. Tests on single waves and the first wave of the multiple-wave model indicated that in turbulent flow the maximum heating on the waves increased almost linearly with decreasing geometric width-height ratio of the waves.

4. The prediction technique employed in this investigation to indicate turbulent maximum heating on a surface protuberance gave fair estimates when there was no boundary-layer separation prior to the wave.

Langley Research Center,
National Aeronautics and Space Administration,
Langley Station, Hampton, Va., October 6, 1967,
129-01-08-41-23.

REFERENCES

1. Burbank, Paige B.; Newlander, Robert A.; and Collins, Ida K.: Heat-Transfer and Pressure Measurements on a Flat-Plate Surface and Heat-Transfer Measurements on Attached Protuberances in a Supersonic Turbulent Boundary Layer at Mach Numbers of 2.65, 3.51, and 4.44. NASA TN D-1372, 1962.

2. Shore, Charles P.; Dixon, Sidney C ; and Griffith, George E.: Experimental Pressures and Turbulent Heat-Transfer Coefficients Associated With Sinusoidal Protuberances on a Flat Plate at a Mach Number of 3. NASA TN D-1626, 1963.

3. Wisniewski, Richard J.: Turbulent Heat-Transfer Coefficients in the Vicinity of Surface Protuberances. NASA MEMO 10-1-58E, 1958.

4. Czarnecki, K. R.; and Monta, William J.: Pressure Distributions and Wave Drag Due to Two-Dimensional Fabrication-Type Surface Roughness on an Ogive Cylinder at Mach Numbers of 1.61 and 2.01. NASA TN D-835, 1961.

5. Bertram, M. H.; Weinstein, L. M.; Cary, A. M., Jr.; and Arrington, J. P.: Effect of Two-Dimensional Multiple-Wave Distortions on the Heat Transfer to a Wall in Hypersonic Flow. AIAA Paper No. 67-164, Jan. 1967.

6. Jaeck, C. L.: Analysis of Pressure and Heat Transfer Tests on Surface Roughness Elements With Laminar and Turbulent Boundary Layers. NASA CR-537, 1966.

7. Bertram, Mitchel H.; and Wiggs, M. Margarette: Effect of Surface Distortions on the Heat Transfer to a Wing at Hypersonic Speeds. AIAA J., vol. 1, no. 6, June 1963, pp. 1313-1319.

8. Rhudy, J. P.; and Magnan, J. D.: Investigation of Heat Transfer and Pressure Distributions in Regions of Surface Distortion on a Flat Plate. AEDC-TDR-62-238, U.S. Air Force, Jan. 1963.

9. Arrington, James P.: Heat Transfer and Pressure Distributions in Regions of Sinusoidal Protuberances on a Flat Plate. M. S. Thesis, Virginia Polytech. Inst., 1966.

10. Dunavant, James C.; and Stone, Howard W.: Effect of Roughness on Heat Transfer to Hemisphere Cylinders at Mach Numbers 10.4 and 11.4. NASA TN D-3871, 1967.

11. Bloom, Martin H.; and Pallone, Adrian: Heat Transfer to Surfaces in the Neighborhood of Protuberances in Hypersonic Flow. WADC TN 57-95, ASTIA Doc. No. AD 118138, U.S. Air Force, Aug. 1957.

12. Sterrett, James R.; and Emery, James C.: Extension of Boundary-Layer-Separation Criteria to a Mach Number of 6.5 By Utilizing Flat Plates With Forward-Facing Steps. NASA TN D-618, 1960.

13. Holloway, Paul F.; and Sterrett, James R.: Effect of Controlled Surface Roughness on Boundary-Layer Transition and Heat Transfer at Mach Numbers of 4.8 and 6.0. NASA TN D-2054, 1964.

14. Monaghan, R. J.: On the Behavior of Boundary Layers at Supersonic Speeds. Fifth International Aeronautical Conference, Rita J. Turino and Caroline Taylor, eds., Inst. Aeron. Sci., Inc., June 1955, pp. 277-315.

15. Hilsenrath, Joseph: The NBS-NACA Tables of Thermal Properties of Gases. Table 2.44 Dry Air – Prandtl Number. Nat. Bur. Std., U.S. Dept. Com., July 1950.

16. Bertram, Mitchel H.; and Everhart, Philip E.: An Experimental Study of the Pressure and Heat-Transfer Distribution on a 70° Sweep Slab Delta Wing in Hypersonic Flow. NASA TR R-153, 1963.

17. Chapman, Dean R.; Kuehn, Donald M.; and Larson, Howard K.: Investigation of Separated Flows in Supersonic and Subsonic Streams With Emphasis on the Effect of Transition. NACA Rept. 1356, 1958.

18. Bertram, Mitchel H.; and Blackstock, Thomas A.: Some Simple Solutions to the Problem of Predicting Boundary-Layer Self-Induced Pressures. NASA TN D-798, 1961.

19. Baradell, Donald L.; and Bertram, Mitchel H.: The Blunt Plate in Hypersonic Flow. NASA TN D-408, 1960.

20. Holloway, Paul F.; Sterrett, James R.; and Creekmore, Helen S.: An Investigation of Heat Transfer Within Regions of Separated Flow at a Mach Number of 6.0. NASA TN D-3074, 1965.

21. Van Driest, E. R.: Investigation of Laminar Boundary Layer in Compressible Fluids Using the Crocco Method. NACA TN 2597, 1952.

22. Nagel, A. L.; Fitzsimmons, H. D.; and Doyle, L. B.: Analysis of Hypersonic Pressure and Heat Transfer Tests on Delta Wings With Laminar and Turbulent Boundary Layers. NASA CR-535, 1966.

23. Bertram, Mitchel H.; and Feller, William V.: A Simple Method for Determining Heat Transfer, Skin Friction, and Boundary-Layer Thickness for Hypersonic Laminar Boundary-Layer Flows in a Pressure Gradient. NASA MEMO 5-24-59L, 1959.

24. Bertram, Mitchel H.; and Neal, Luther, Jr.: Recent Experiments in Hypersonic Turbulent Boundary Layers. Presented to the AGARD Specialists Meeting on Recent Developments in Boundary-Layer Research (Naples, Italy), May 10-14, 1965.

25. Schlichting, Hermann: Boundary Layer Theory. Fourth ed., McGraw-Hill Book Co., Inc., c.1960.

26. Spalding, D. B.; and Chi, S. W.: The Drag of a Compressible Turbulent Boundary Layer on a Smooth Flat Plate With and Without Heat Transfer. J. Fluid Mech., vol. 18, pt. 1, Jan. 1964, pp. 117-143.

27. Persh, Jerome; and Lee, Roland: Tabulation of Compressible Turbulent Boundary Layer Parameters. NAVORD Rept. 4282 (Aeroballistic Res. Rept. 337), U.S. Naval Ord. Lab., May 1, 1956.

28. Adcock, Jerry B.; Peterson, John B., Jr.; and McRee, Donald I.: Experimental Investigation of a Turbulent Boundary Layer at Mach 6, High Reynolds Numbers, and Zero Heat Transfer. NASA TN D-2907, 1965.

29. Arrington, James P.; Molloy, John K.; and Goldberg, Theodore J.: Flare-Stabilization Problems at Hypersonic Mach Numbers. AIAA Sounding Rocket Vehicle Technology Specialist Conference, Feb.-Mar. 1967, pp. 84-91.

TABLE I.- LOCATION OF MODEL INSTRUMENTATION FOR THE MULTIPLE-WAVE PLATES

[L = 40.6 cm]

Thermocouple locations			
Thermocouple	x/L ref. to sharp L.E.	Thermocouple	x/L ref. to sharp L.E.
T1	0.0748	T47	0.3250
T2	.1050	T48	.3363
T3	.1362	T49	.3438
T4	.1675	T50	.3575
T5	.1988	T51	.3688
T6	.1988	T52	.3825
T7	.1988	T53	.4075
T8	.2300	T54	.4188
T9	.2612	T55	.4300
T10	.2915	T56	.4514
T11	.3238	T57	.4625
T12	.3550	T58	.4764
T13	.3864	T59	.5010
T14	.4175	T60	.5063
T15	.4487	T61	.5125
T16	.4487	T62	.5238
T17	.4487	T63	.5315
T18	.4802	T64	.5450
T19	.5110	T65	.5563
T20	.5425	T66	.5698
T21	.5738	T67	.5698
T22	.6365	T68	.5698
T23	.6985	T69	.5950
T24	.7614	T70	.6063
T25	.8235	T71	.6173
T26	.8860	T72	.6490
T27	.8860	T73	.6500
T28	.8860	T74	.6638
T29	.8860	T75	.6890
T30	.9490	T76	.6940
T31	.0662	T77	.7000
T32	.0975	T78	.7110
T33	.1294	T79	.7190
T34	.1607	T80	.7376
T35	.1767	T81	.7530
T36	.1918	T82	.7690
T37	.2075	T83	.7845
T38	.2075	T84	.8158
T39	.2075	T85	.8470
T40	.2232	T86	.8780
T41	.2388	T87	.9095
T42	.2700	T88	.9410
T43	.2857	T89	.9718
T44	.3013	T90	.9718
T45	.3138	T91	.9718
T46	.3178	T92	.9718

Pressure-orifice locations			
Pressure orifice	x/L ref. to sharp L.E.	Pressure orifice	x/L ref. to sharp L.E.
P1	0.0432	P33	0.4300
P2	.0903	P34	.4513
P3	.1368	P35	.4625
P4	.1994	P36	.4762
P5	.2619	P37	.5010
P6	.3245	P38	.5125
P7	.4495	P39	.5238
P8	.4495	P40	.5450
P9	.4495	P41	.5450
P10	.5744	P42	.5450
P11	.6993	P43	.5563
P12	.8240	P44	.5698
P13	.8860	P45	.5950
P14	.8860	P46	.6063
P15	.8860	P47	.6173
P16	.9490	P48	.6490
P17	.1594	P49	.6500
P18	.1751	P50	.6638
P19	.2063	P51	.6890
P20	.2218	P52	.7000
P21	.2375	P53	.7110
P22	.2688	P54	.7260
P23	.2844	P55	.7428
P24	.3000	P56	.7577
P25	.3138	P57	.7890
P26	.3187	P58	.8202
P27	.3363	P59	.8514
P28	.3575	P60	.8830
P29	.3687	P61	.9140
P30	.3824	P62	.9450
P31	.4075	P63	.9450
P32	.4187	P64	.9450
		P65	.9765

TABLE II.- THERMOCOUPLE LOCATION ON THE SINGLE-WAVE INSERTS

[L = 40.6 cm]

x/L for –			
Plate 1	Plate 2	Plate 3	Plate 4
0.291	0.366	0.366	0.366
.341	.416	.416	.416
.391	.466	.466	.466
.441	.516	.516	.516
.491	.566	.566	.553
.541	.591	.591	.578
.591	.616	.616	.603
.641	.628	.628	.628
.691	.641	.641	.641
.741	.654	.654	.654
.791	.666	.666	.666
.841	.678	.678	.678
.891	.684	.684	.691
	.691	.691	.697
	.697	.697	.704
	.704	.704	.710
	.710	.710	.716
	.716	.716	.722
	.722	.722	.728
	.728	.728	.735
	.741	.741	.741
	.753	.753	.747
	.766	.766	.753
	.778	.778	.766
	.791	.791	.778
	.804	.804	.791
	.816	.841	.816
			.841
			.866
			.891

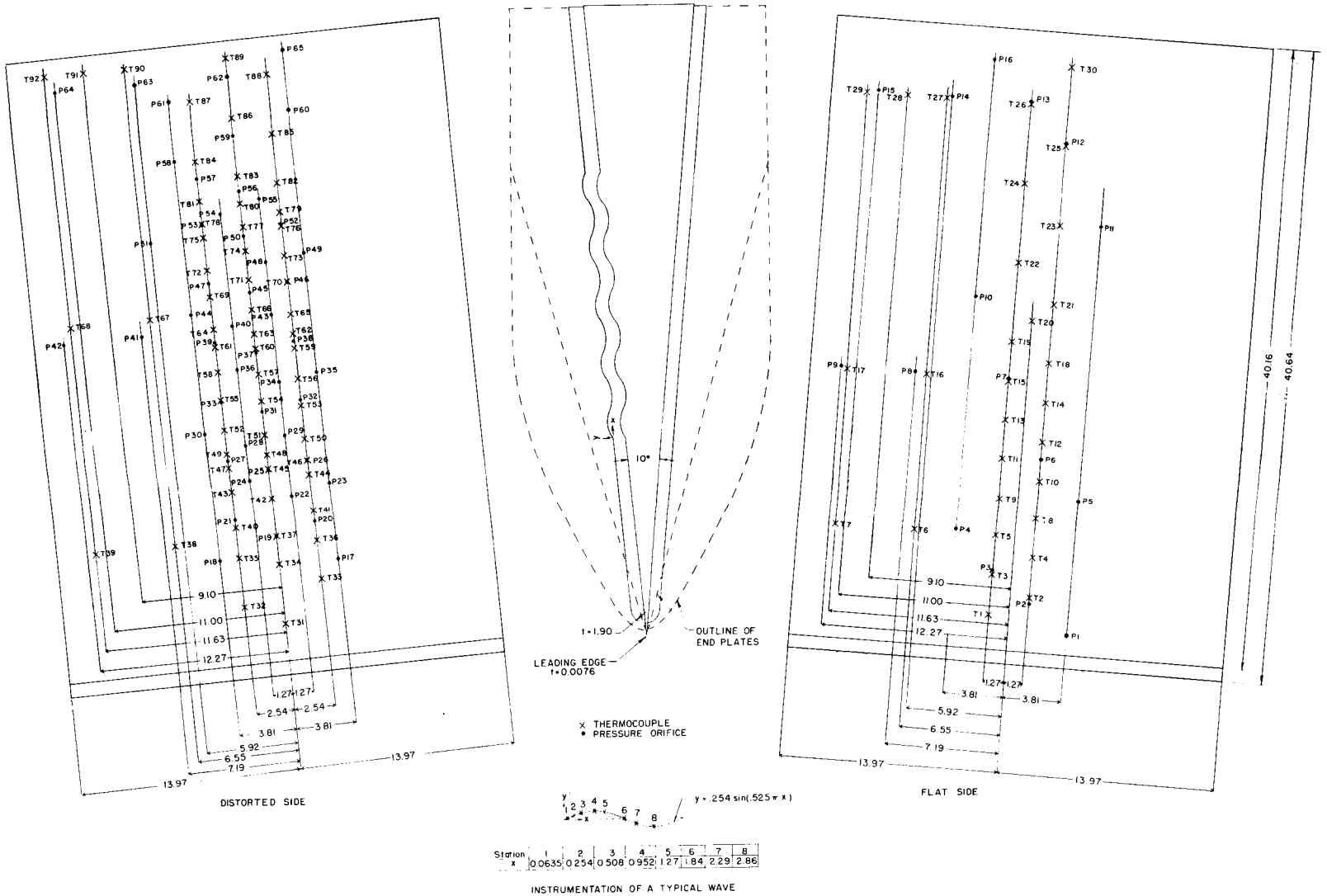

Figure 1.- Multiple-wave model dimensions and instrumentation. All dimensions are in centimeters.

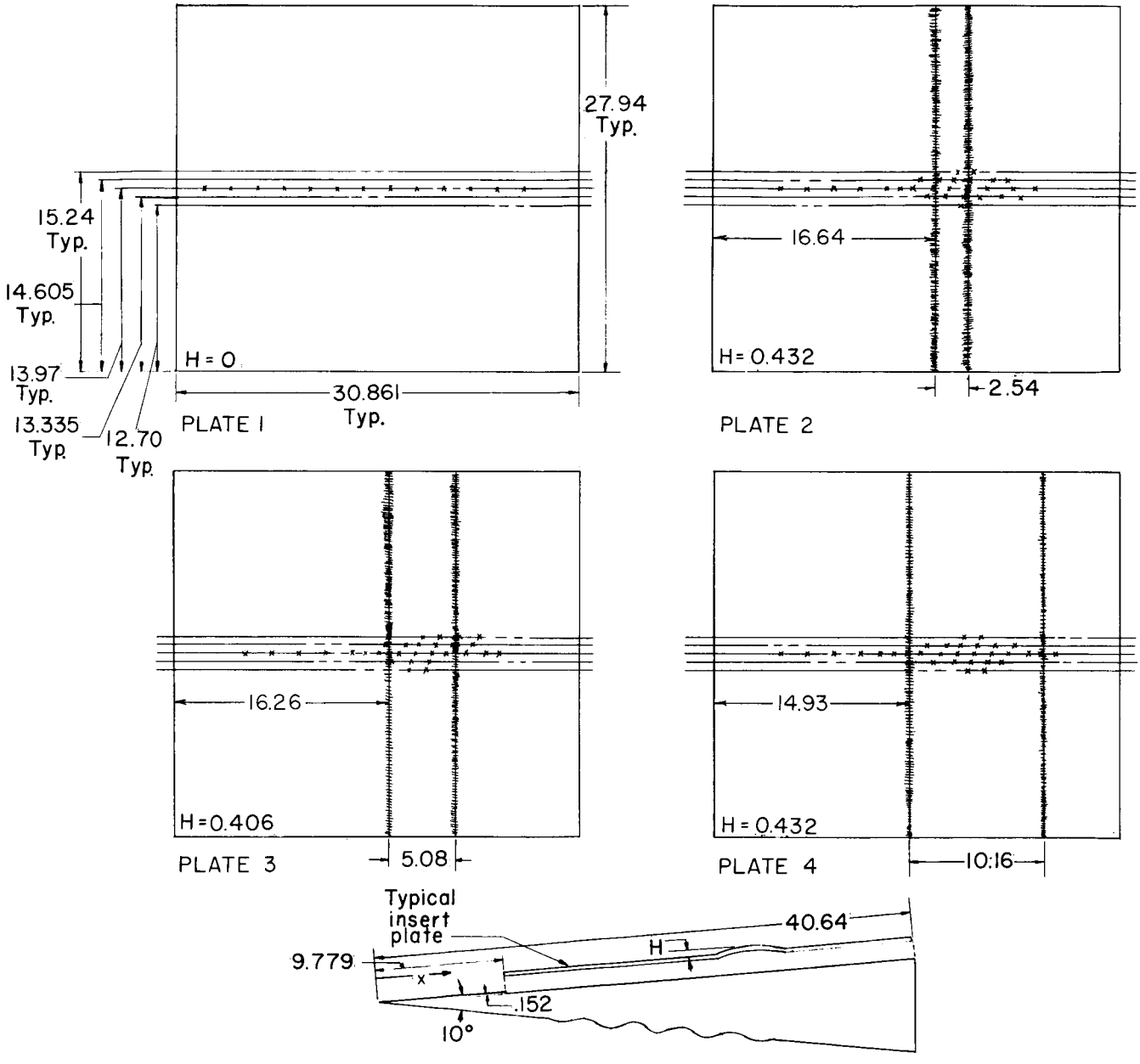

Figure 2.- Model dimensions and instrumentation for the single-wave tests. All dimensions are in centimeters.

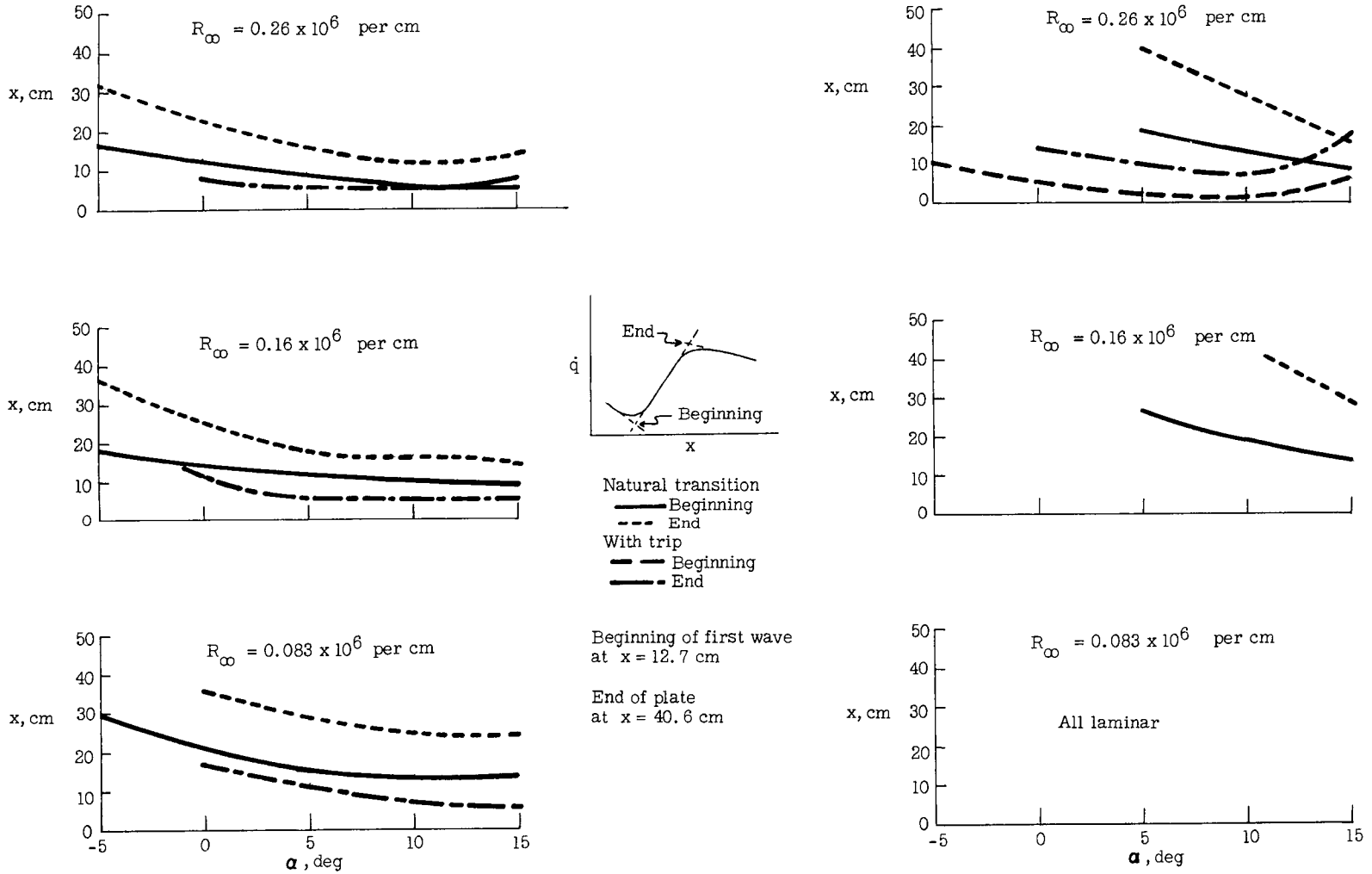

(a) Sharp leading edge.

(b) Blunt leading edge.

Figure 3.- Location of boundary-layer transition for the smooth flat plate as determined from heating data. M_∞ = 6.

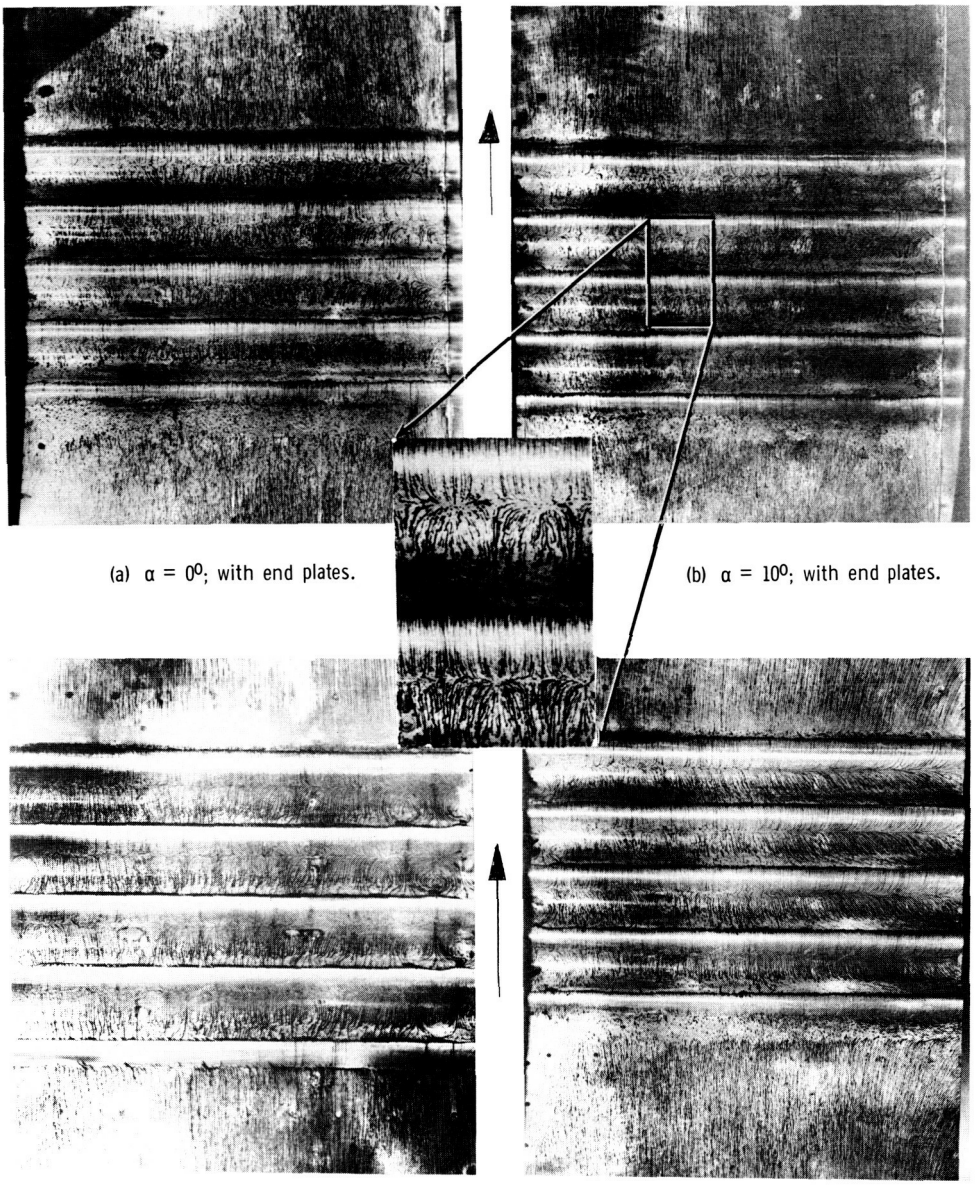

(a) $\alpha = 0^{0}$; with end plates.

(b) $\alpha = 10^{0}$; with end plates.

(c) $\alpha = 15^{0}$; with end plates.

(d) $\alpha = 10^{0}$; right end plate missing.

L-67-8719

Figure 4.- Typical oil-flow patterns for the sine-wave surface with a blunt leading edge. $M_{\infty} = 6$; $R_{\infty}/cm = 0.26 \times 10^{6}$. Arrow indicates flow direction.

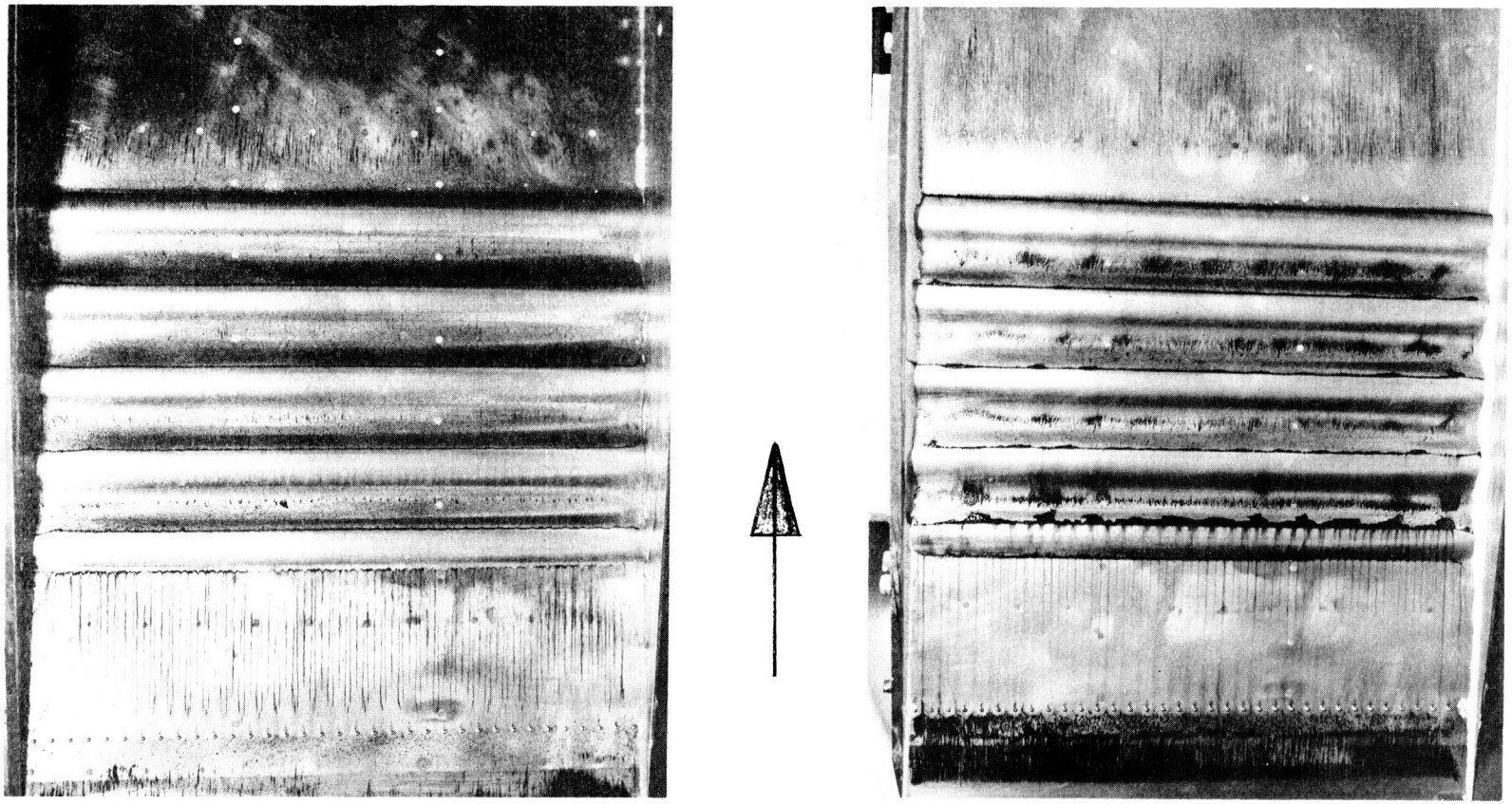

(a) $\alpha = 0^{0}$; with end plates.

(b) $\alpha = 15^{0}$; with end plates. L-67-8720

Figure 5.- Typical oil-flow patterns for the multiple-wave surface with a sharp leading edge and surface roughness. $M_{\infty} = 6$; $R_{\infty}/cm = 0.26 \times 10^{6}$. Arrow indicates flow direction.

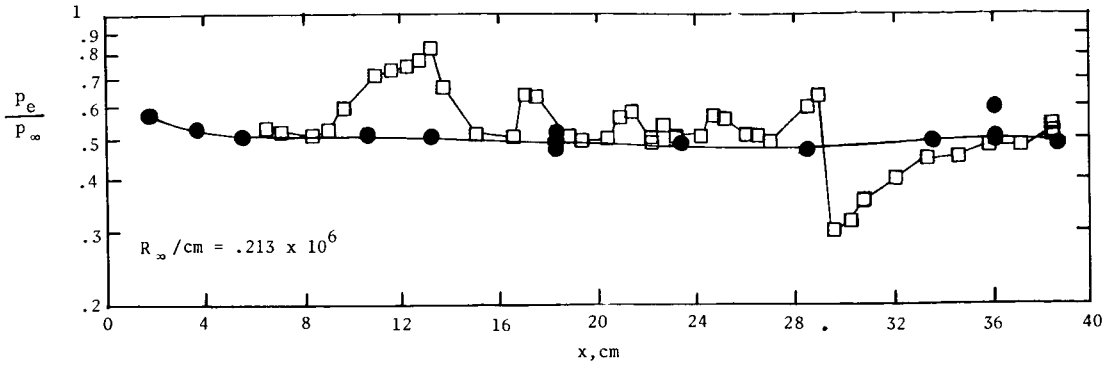

(a) $\alpha = -5^0$.

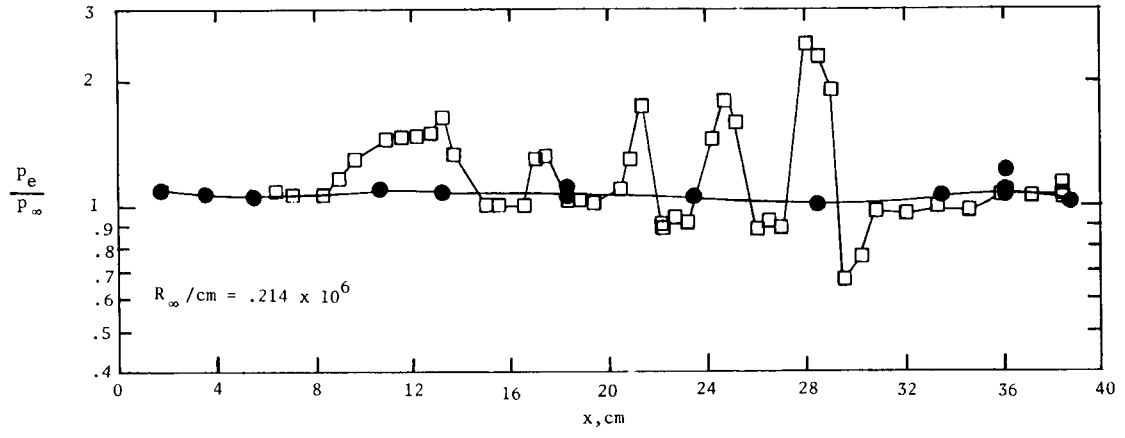

(b) $\alpha = 0^0$.

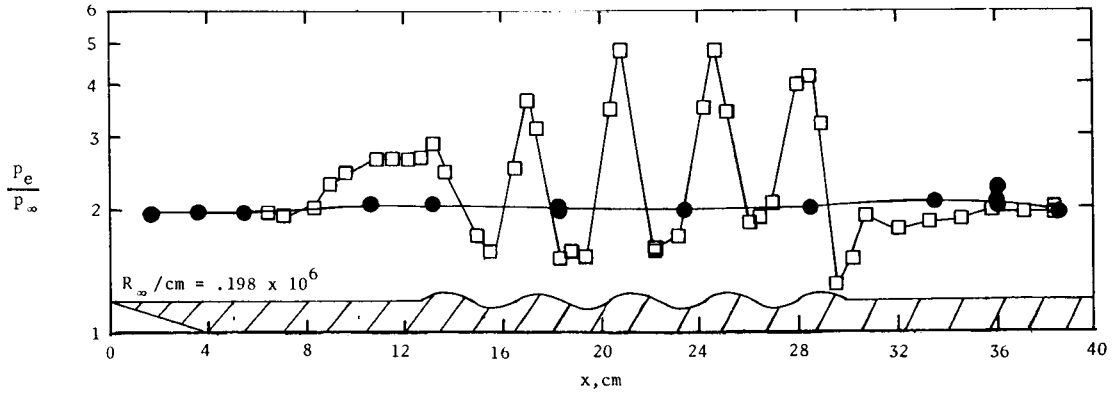

(c) $\alpha = 5^0$.

Figure 6.- Effect of multiple-sine-wave protuberances on the surface pressure for the sharp-leading-edge model. $M_\infty = 6$. Open symbols, multiple-wave surface; solid symbols, flat surface.

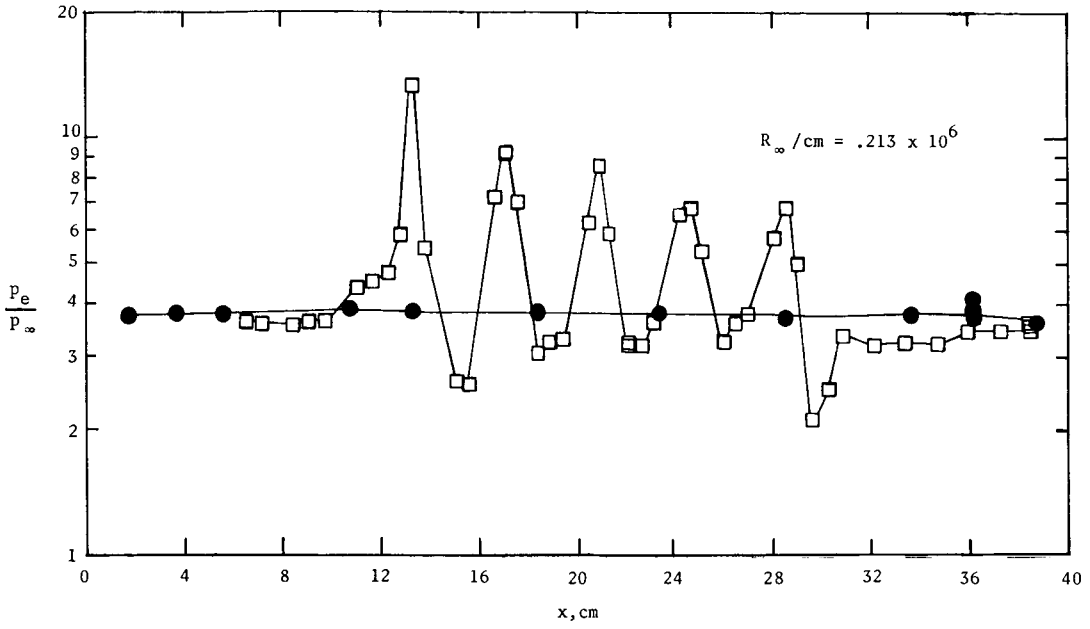

(d) $\alpha = 10^0$.

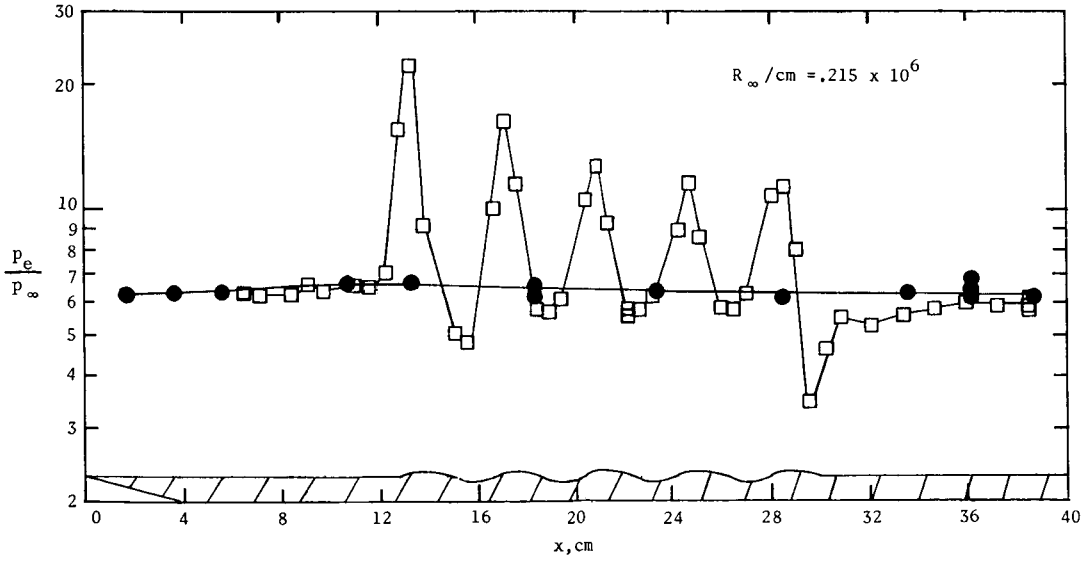

(e) $\alpha = 15^0$.

Figure 6.- Concluded.

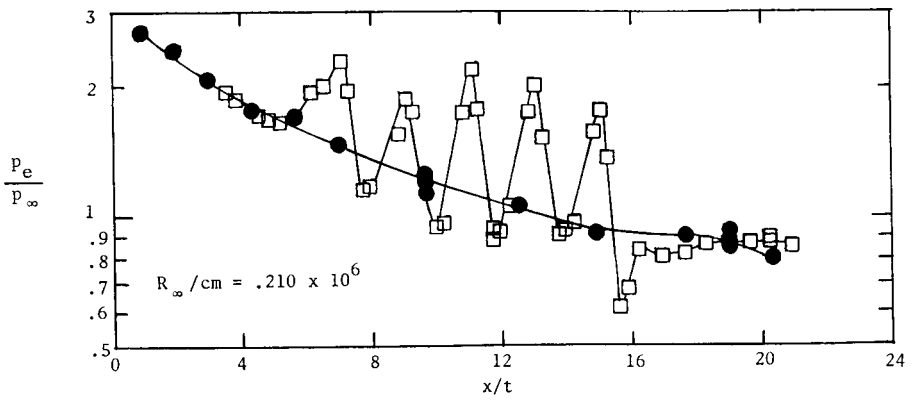

(a) $\alpha = -5^0$.

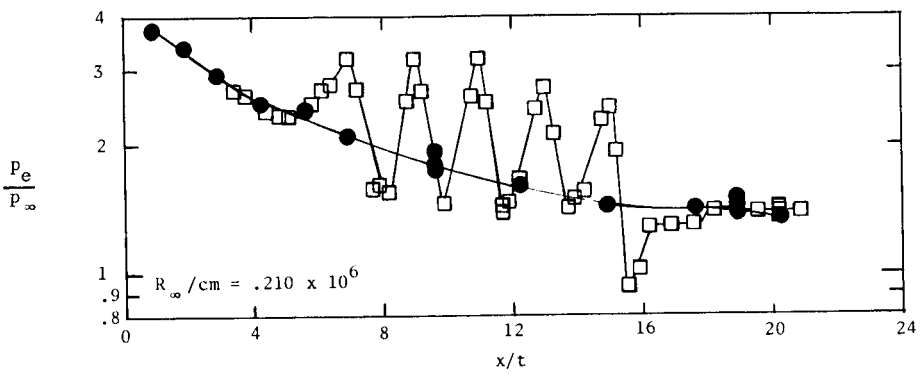

(b) $\alpha = 0^0$.

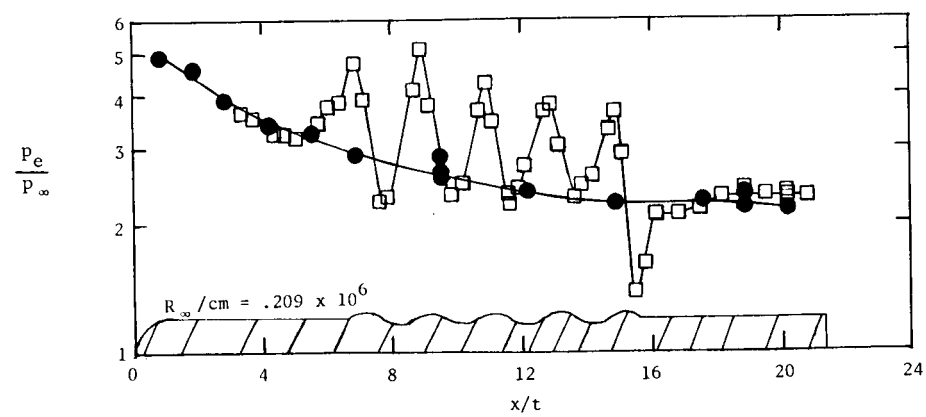

(c) $\alpha = 5^0$.

Figure 7.- Effect of multiple-sine-wave protuberances on the surface pressure for the blunt-leading-edge model. $M_\infty = 6$. Open symbols, multiple-wave surface; solid symbols, flat surface.

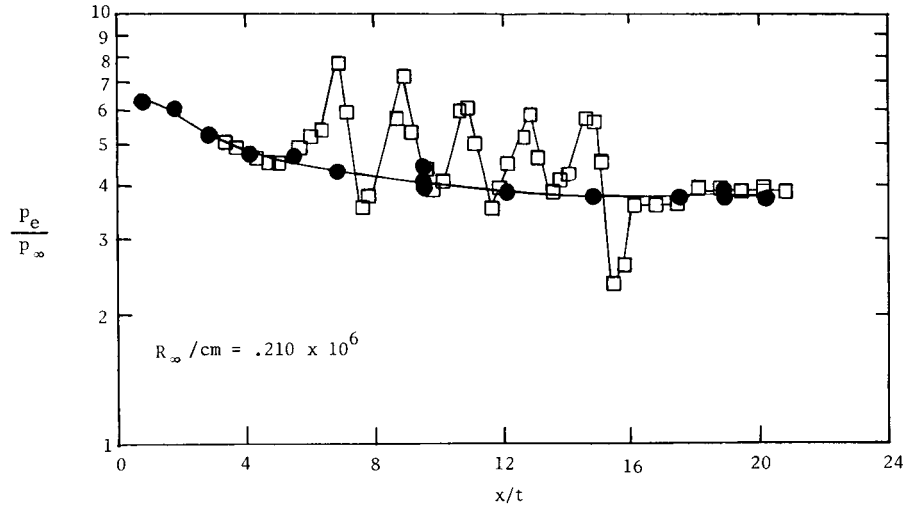

(d) $\alpha = 10^0$.

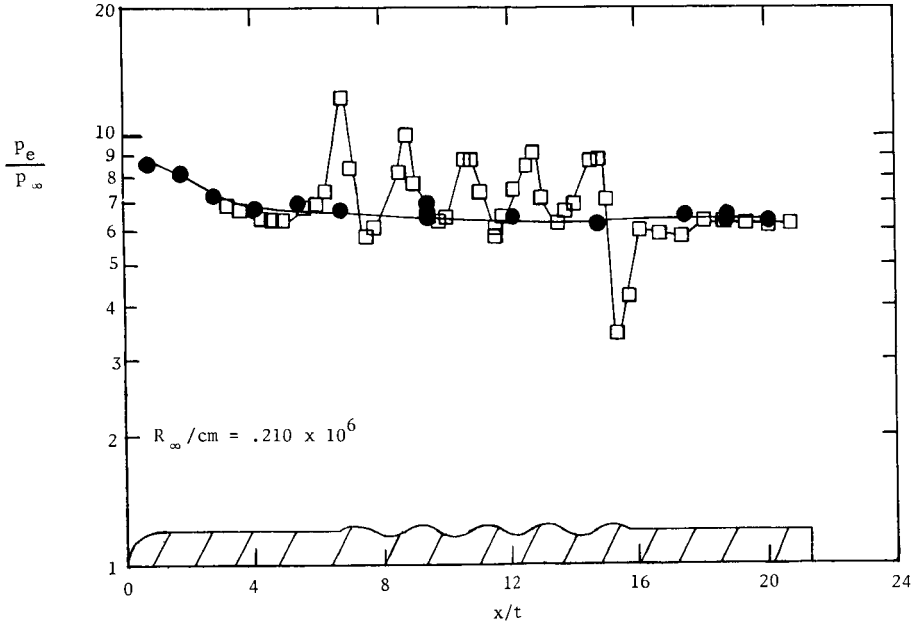

(e) $\alpha = 15^0$.

Figure 7.- Concluded.

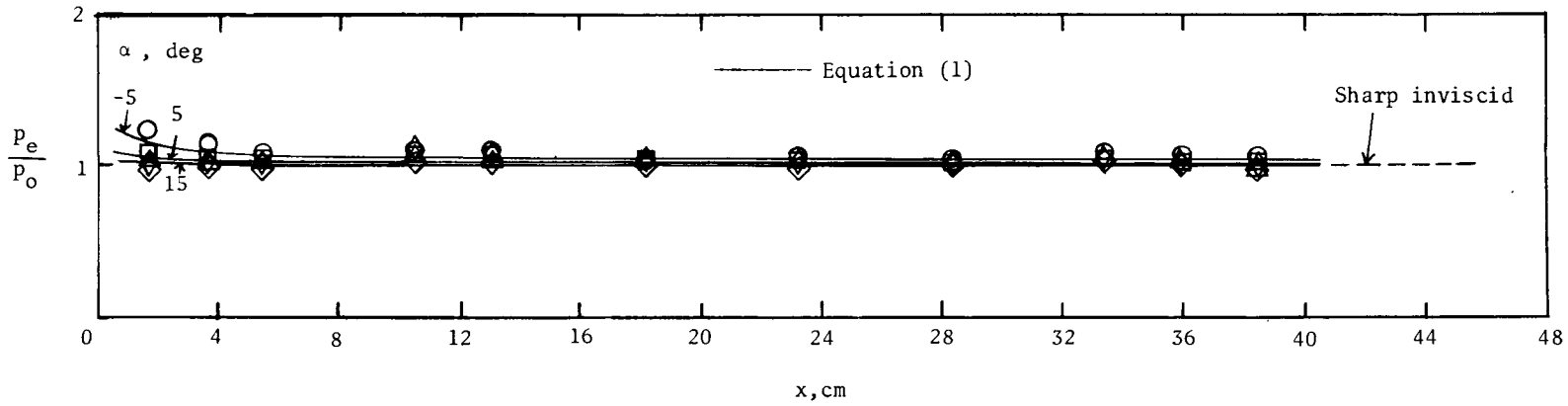

(a) Sharp-leading-edge plate.

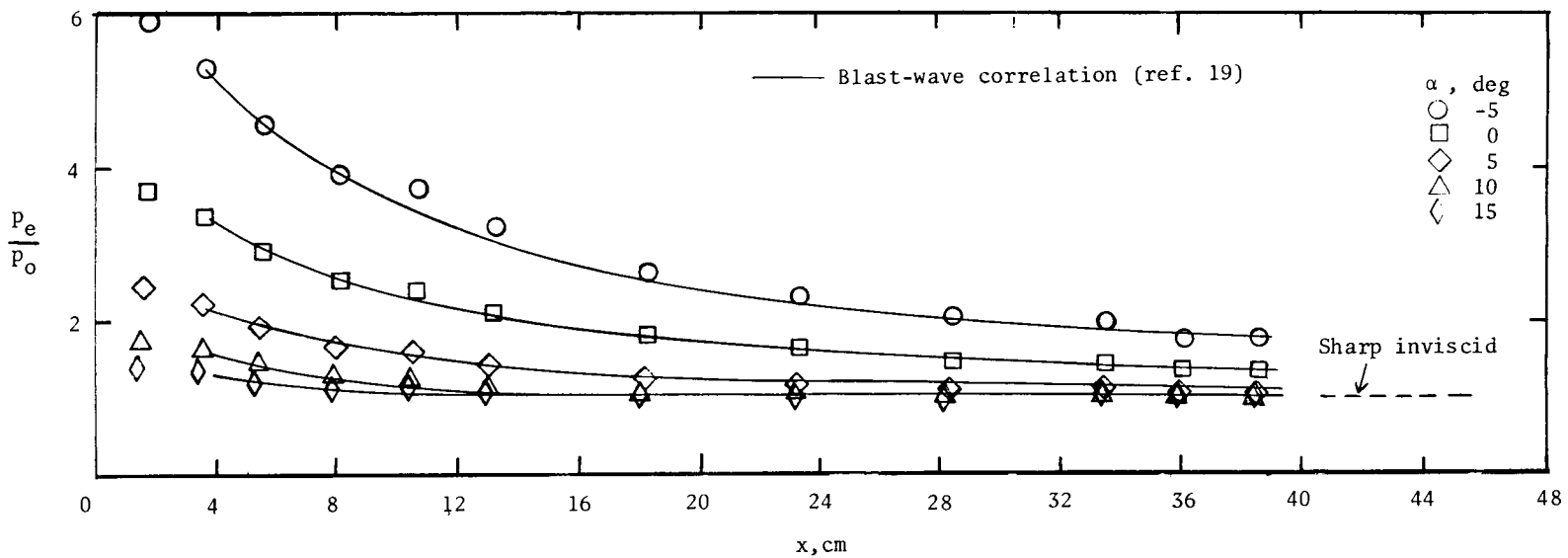

(b) Blunt-leading-edge plate.

Figure 8.- Smooth-plate pressure distributions.

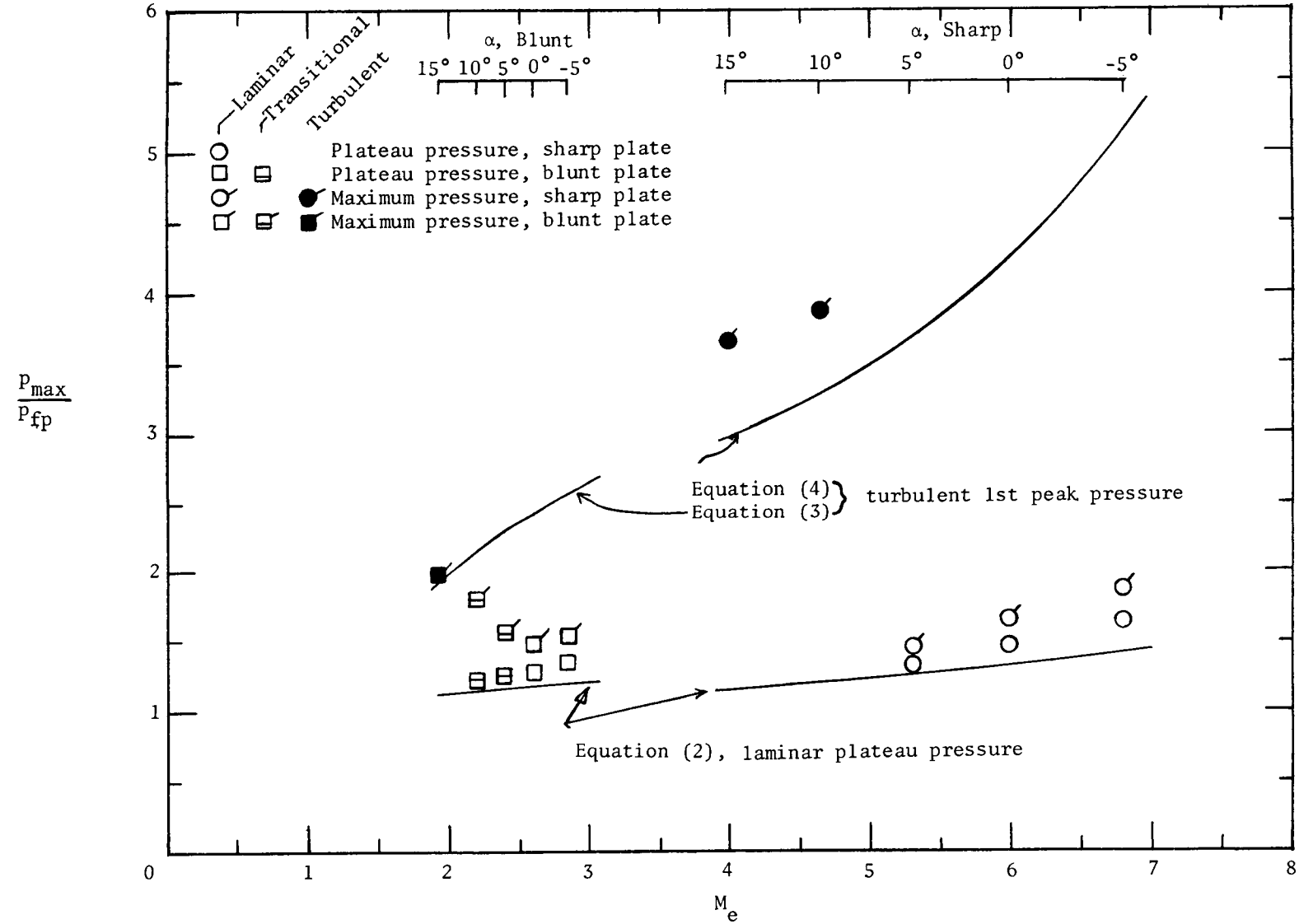

Figure 9.- Maximum and plateau pressures obtained on first wave.

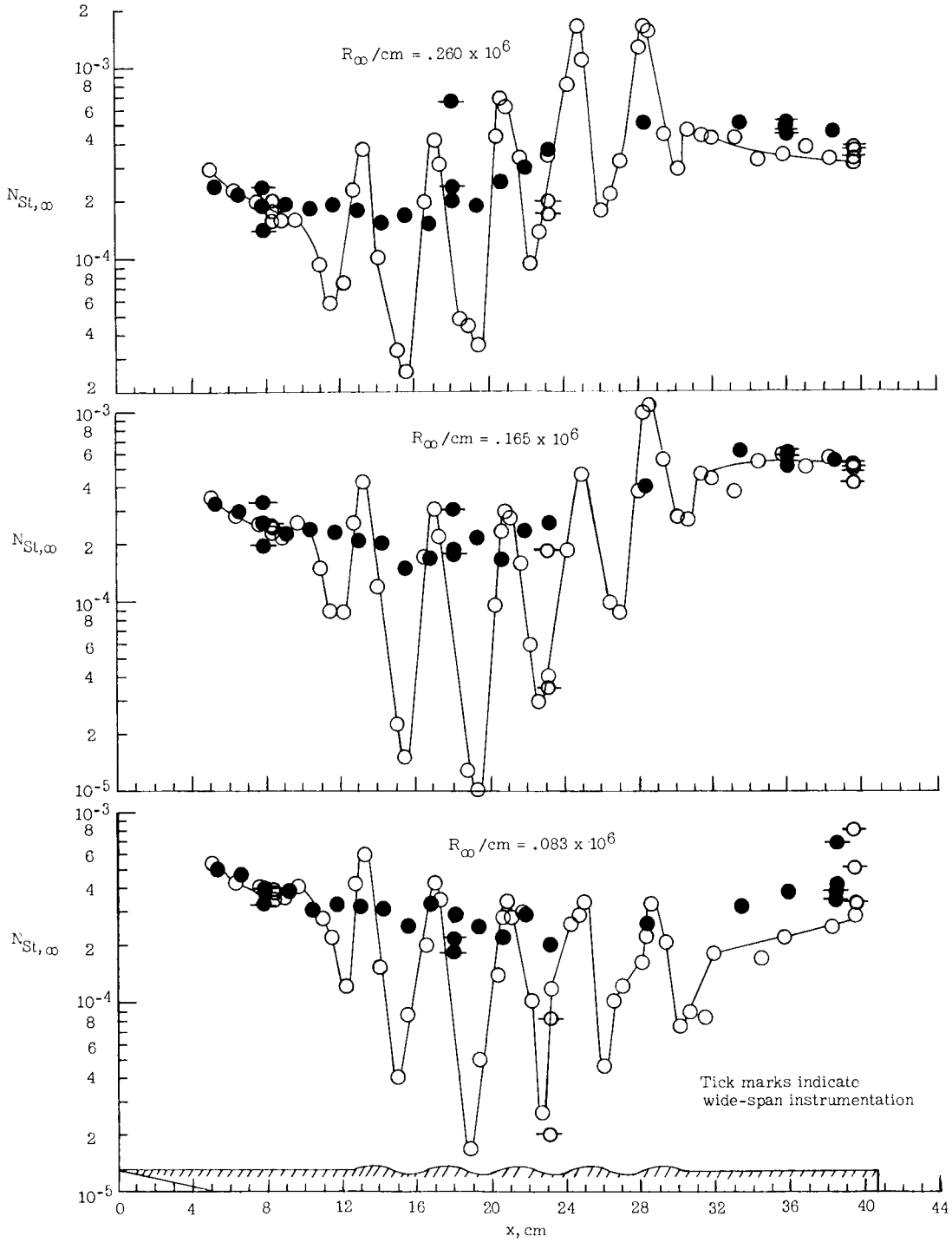

(a) $\alpha = -5^0$.

Figure 10.- Effect of multiple-sine-wave protuberances on surface heating for the sharp-leading-edge model. $M_\infty = 6$. Open symbols, multiple-wave surface; solid symbols, flat surface.

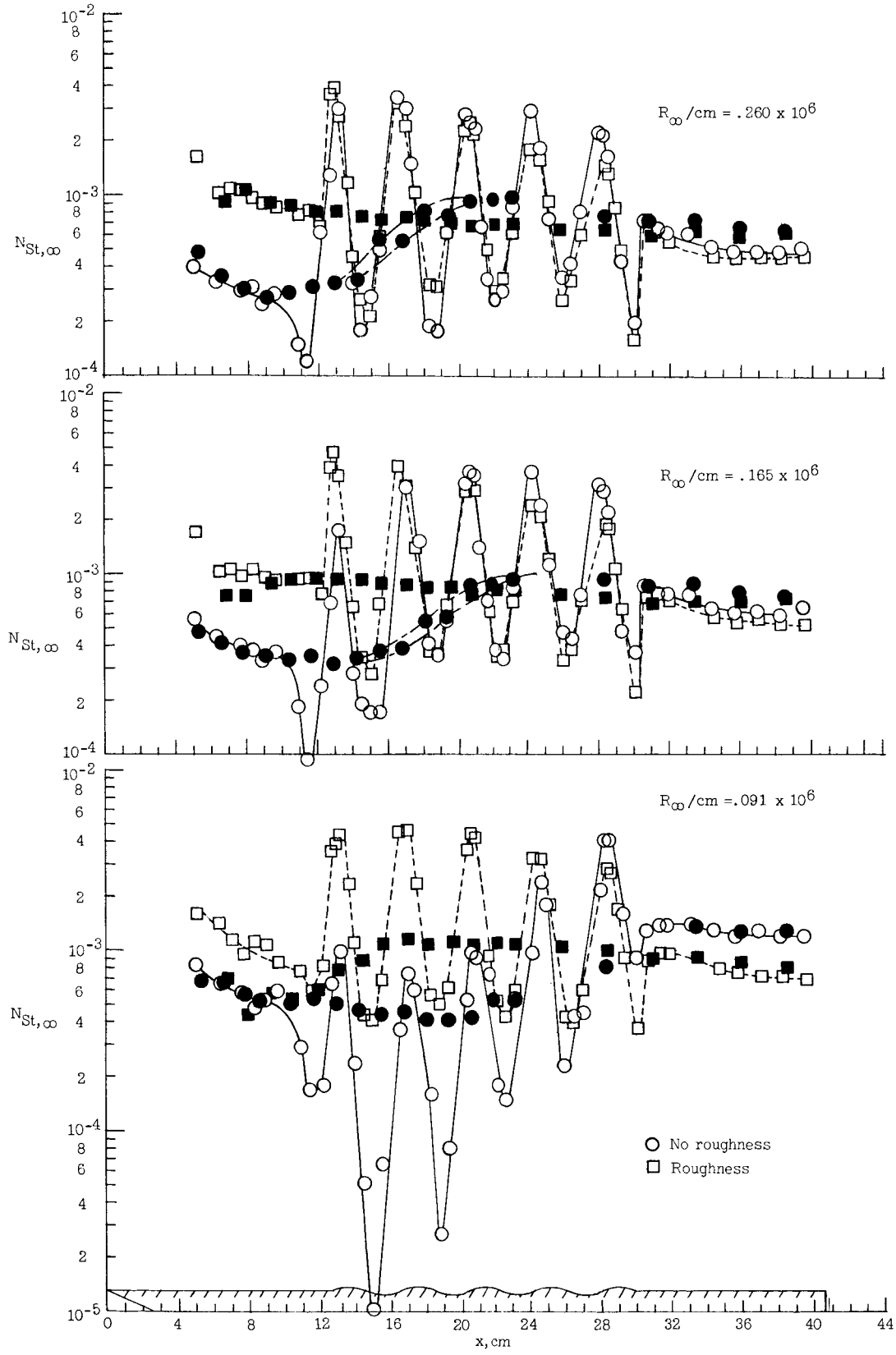

(b) $\alpha = 0^0$.

Figure 10.- Continued.

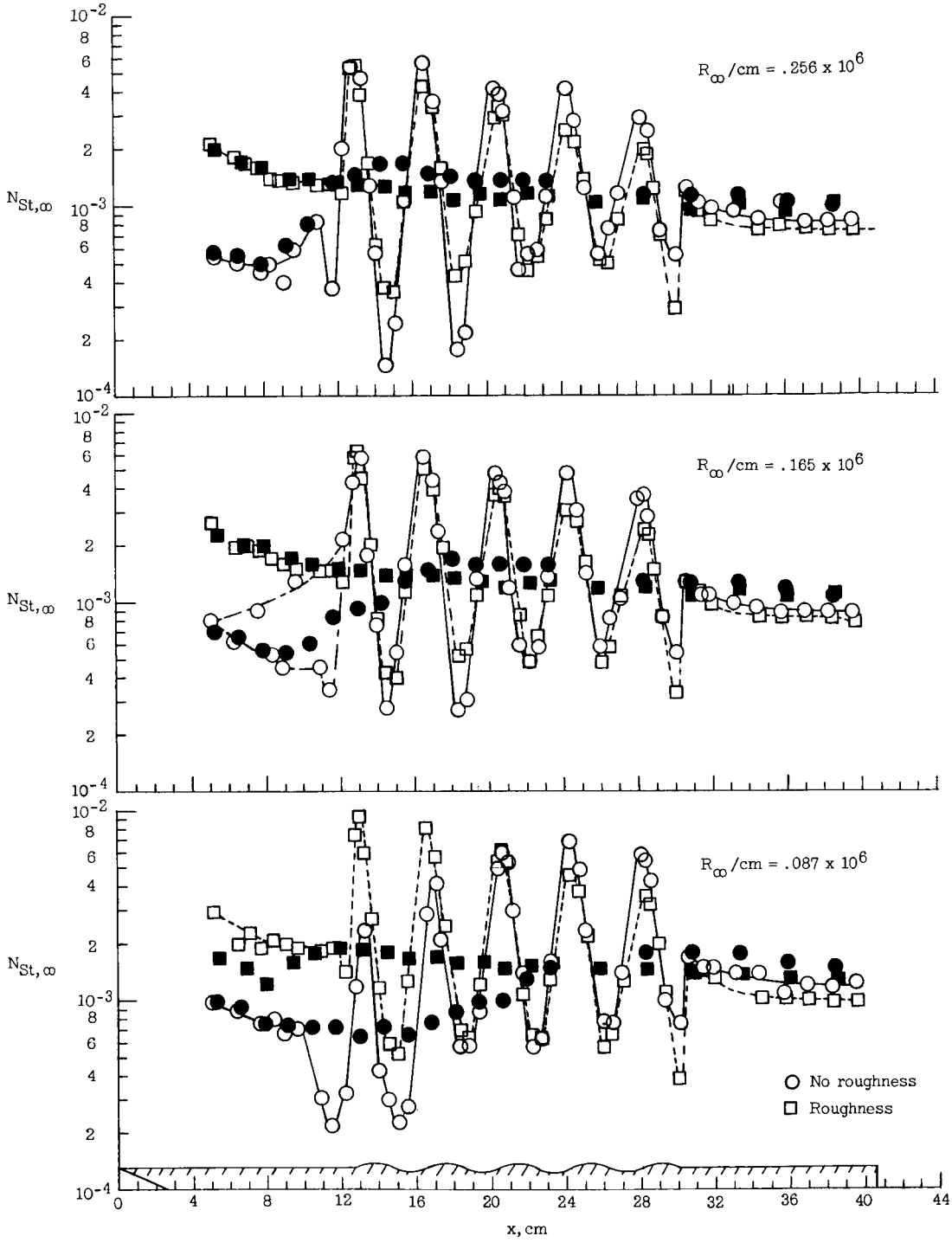

(c) $\alpha = 5^0$.

Figure 10.- Continued.

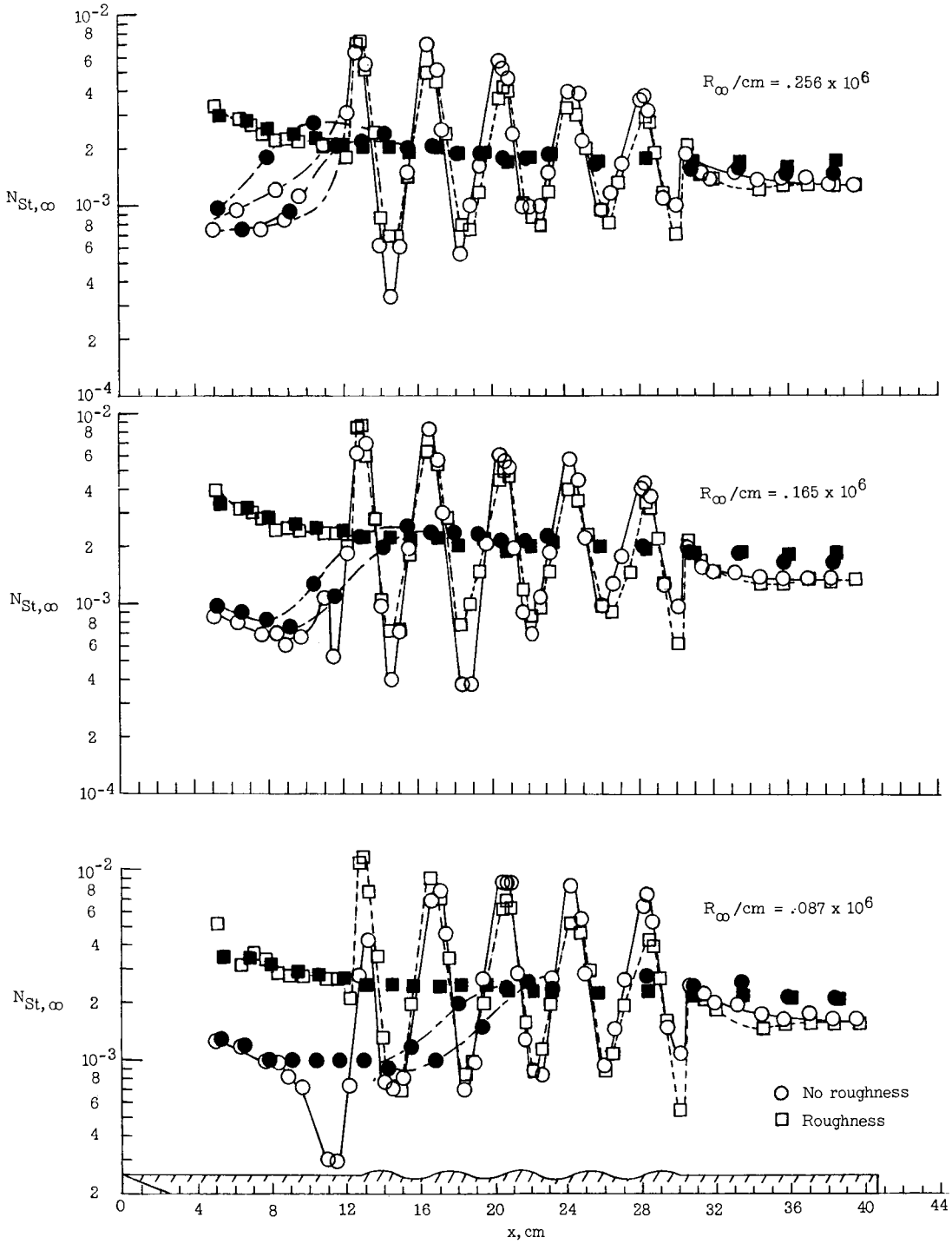

(d) $\alpha = 10^0$.

Figure 10.- Continued.

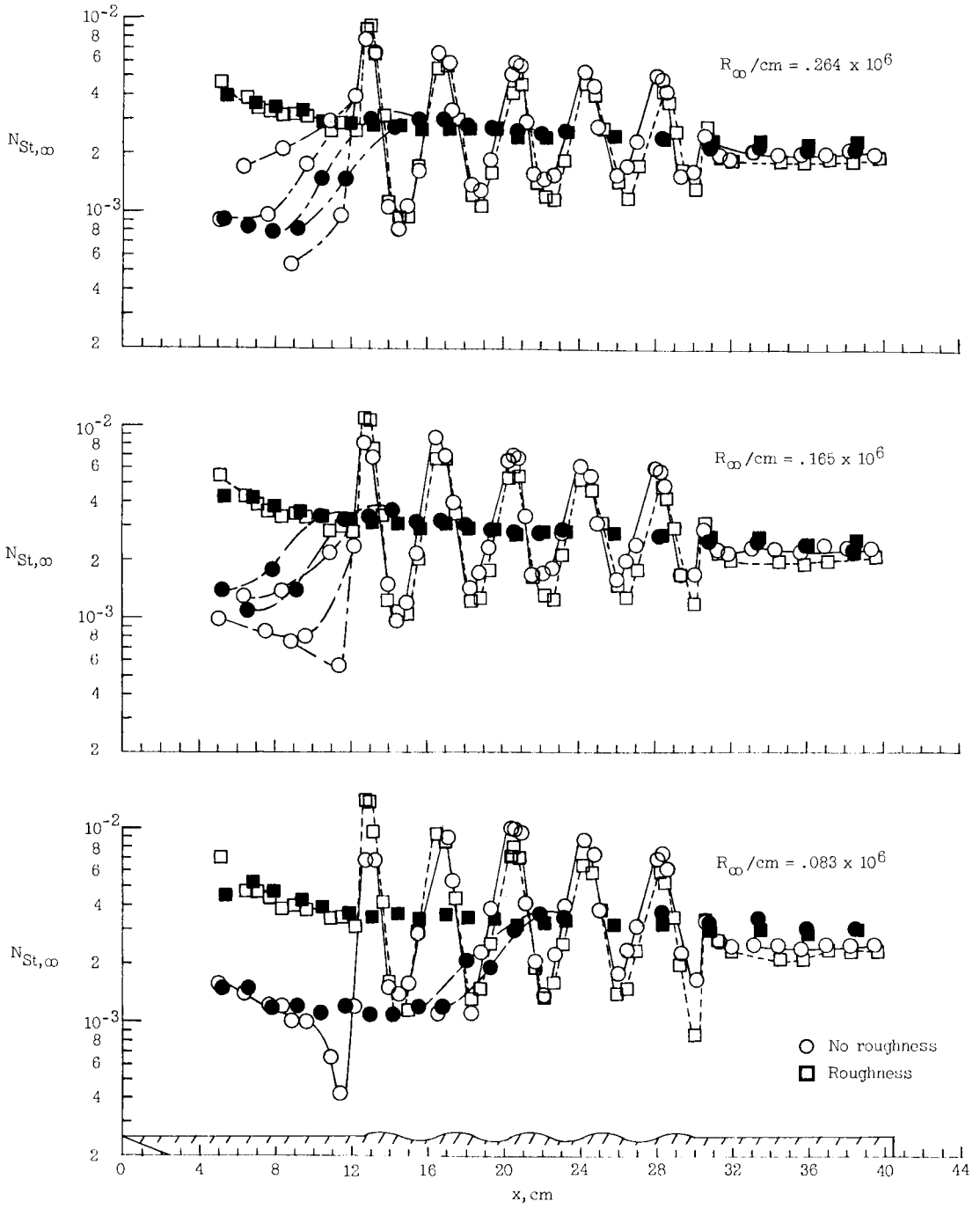

(e) $\alpha = 15^0$.

Figure 10.- Concluded.

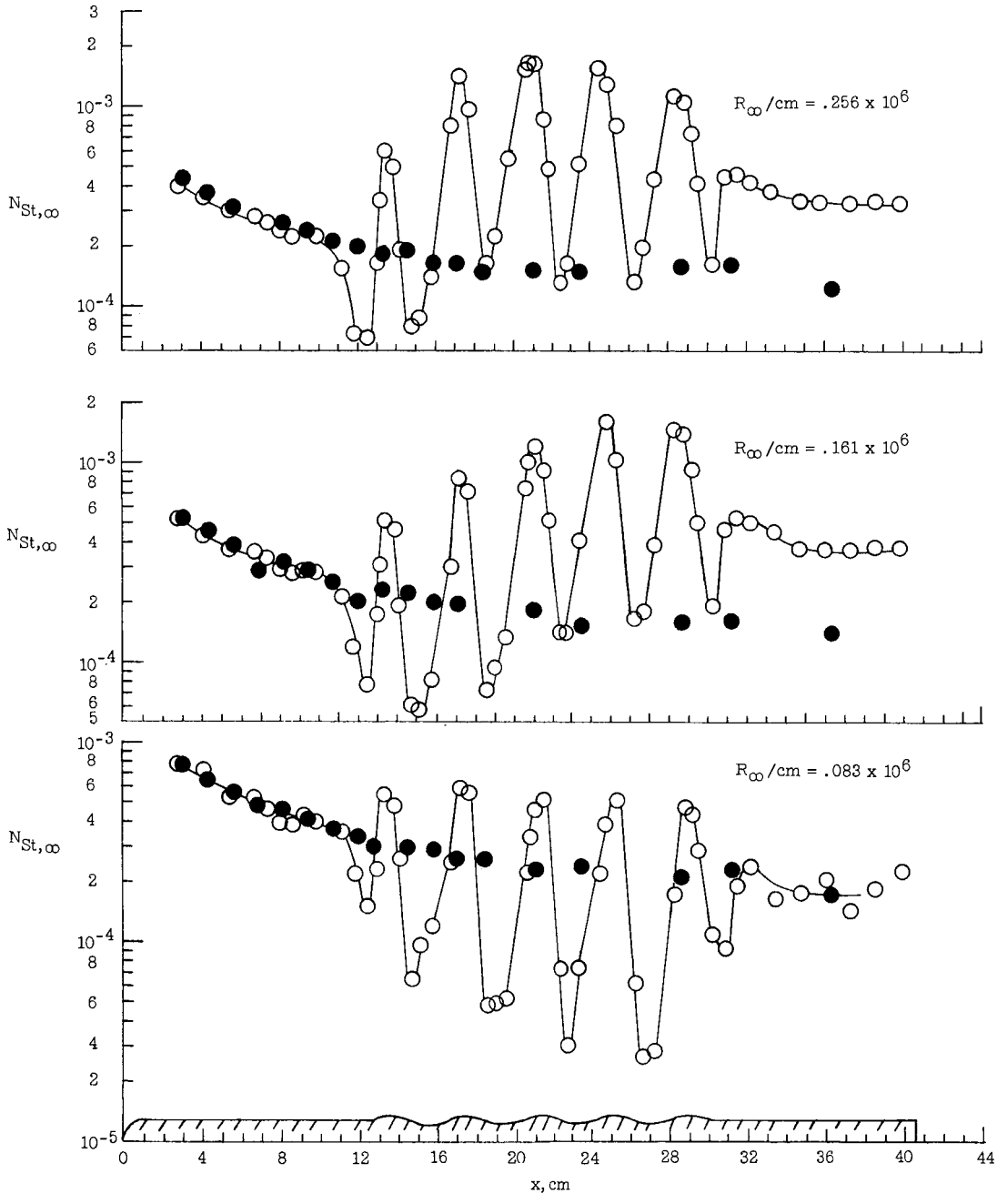

(a) $\alpha = -5^0$.

Figure 11.- Effect of multiple-sine-wave protuberances on surface heating for the blunt-leading-edge model. $M_\infty = 6$. Open symbols, multiple-wave surface; solid symbols, flat surface.

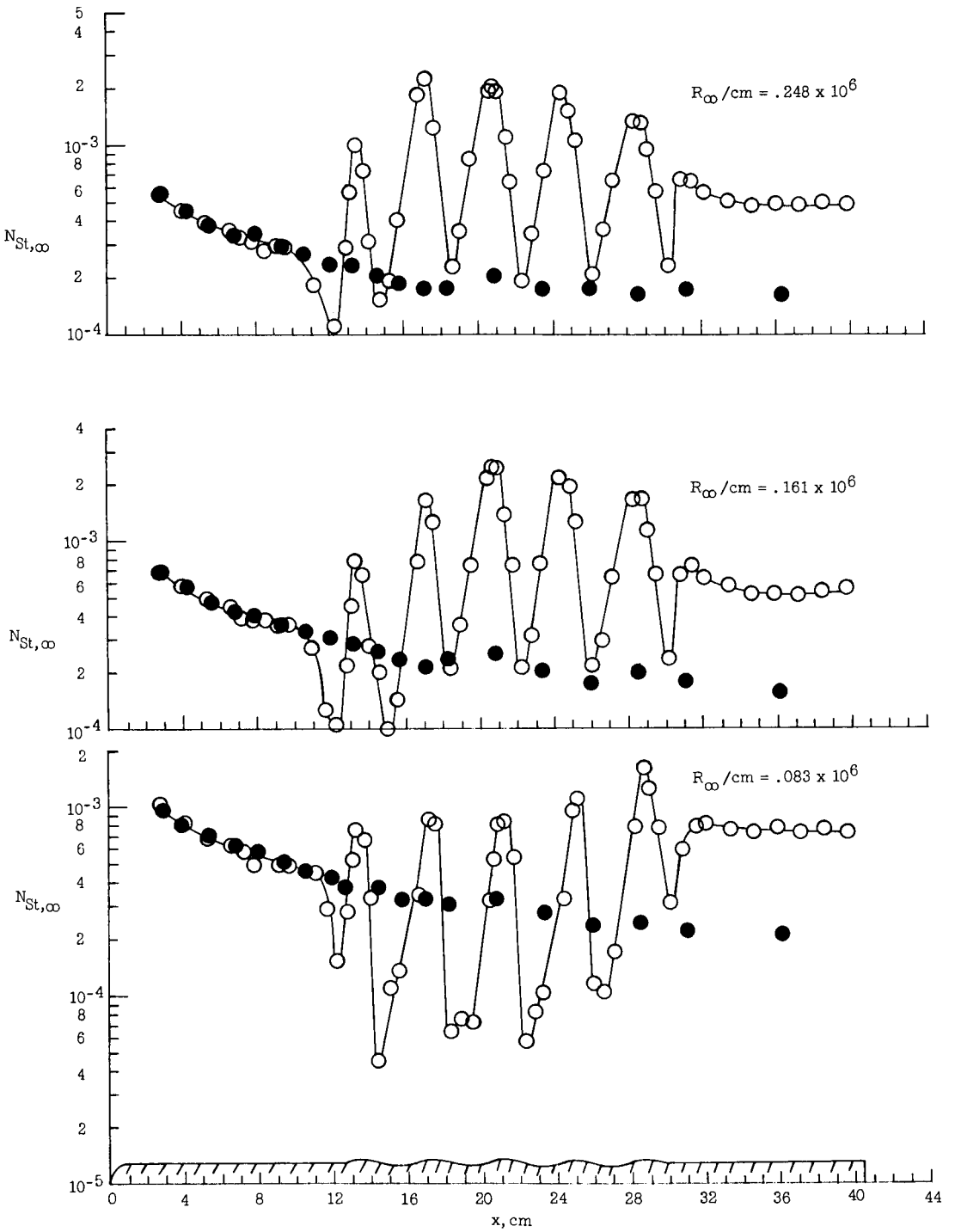

(b) $\alpha = 0^0$.

Figure 11.- Continued.

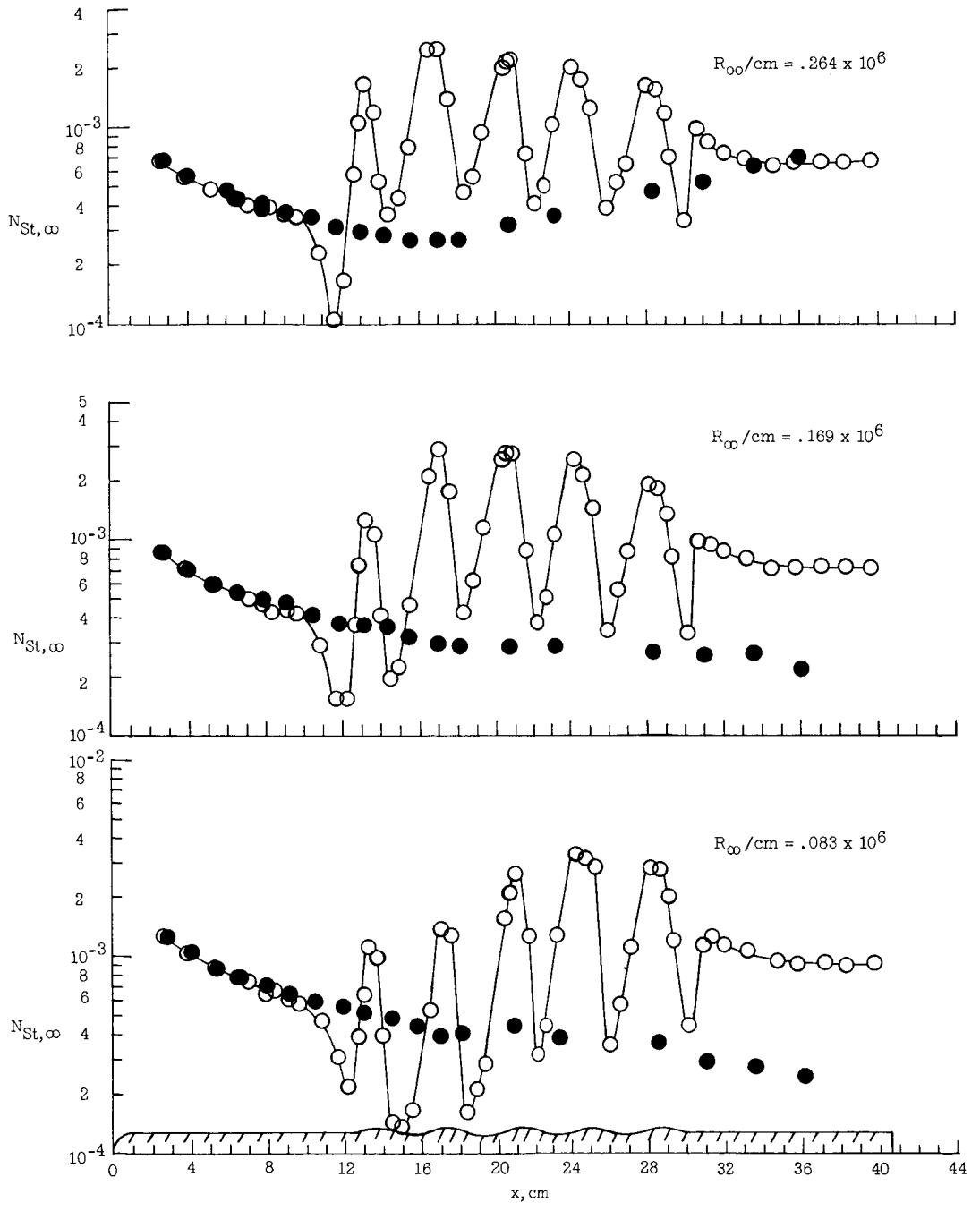

(c) $\alpha = 5^0$.

Figure 11.- Continued.

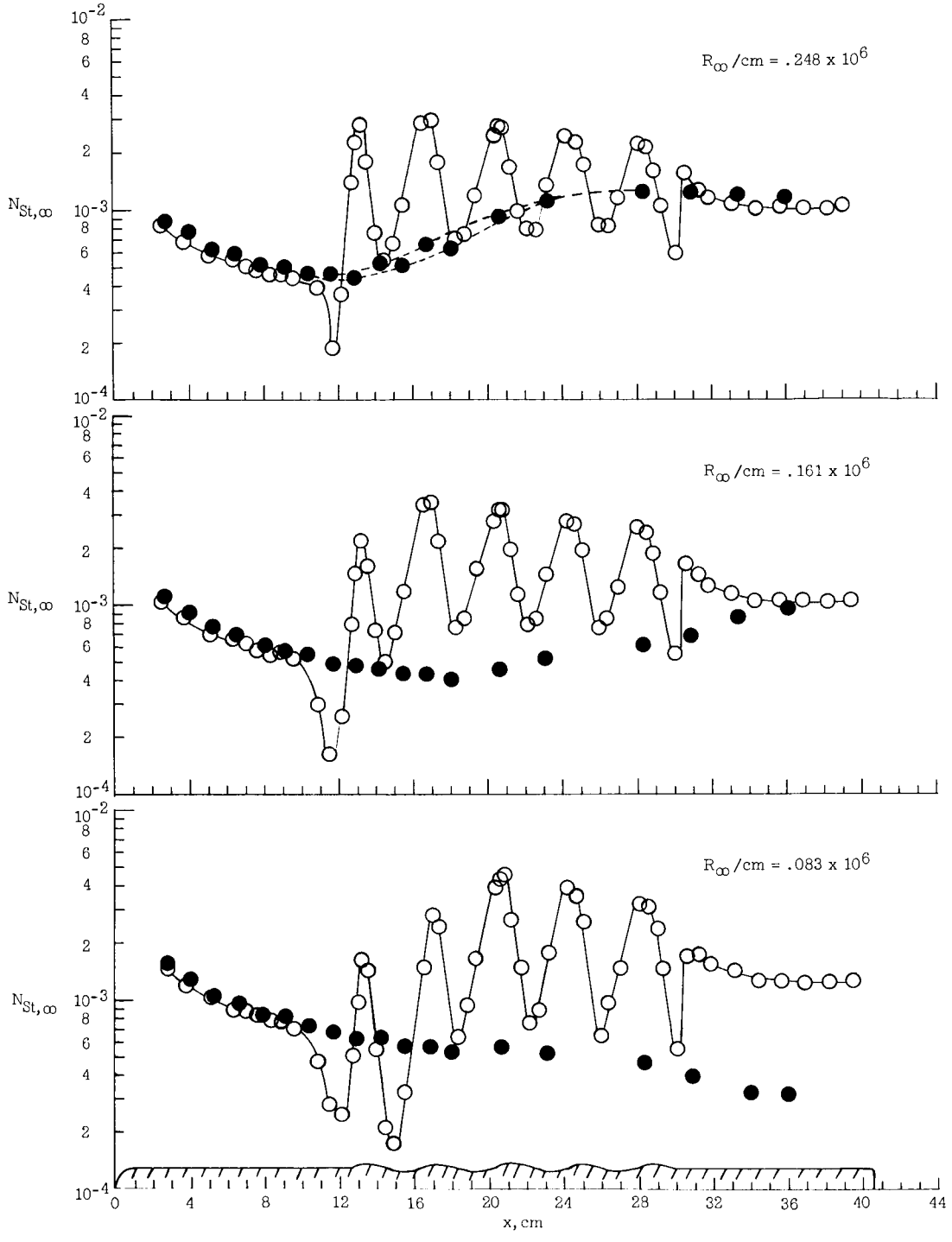

(d) $\alpha = 10^0$.

Figure 11.- Continued.

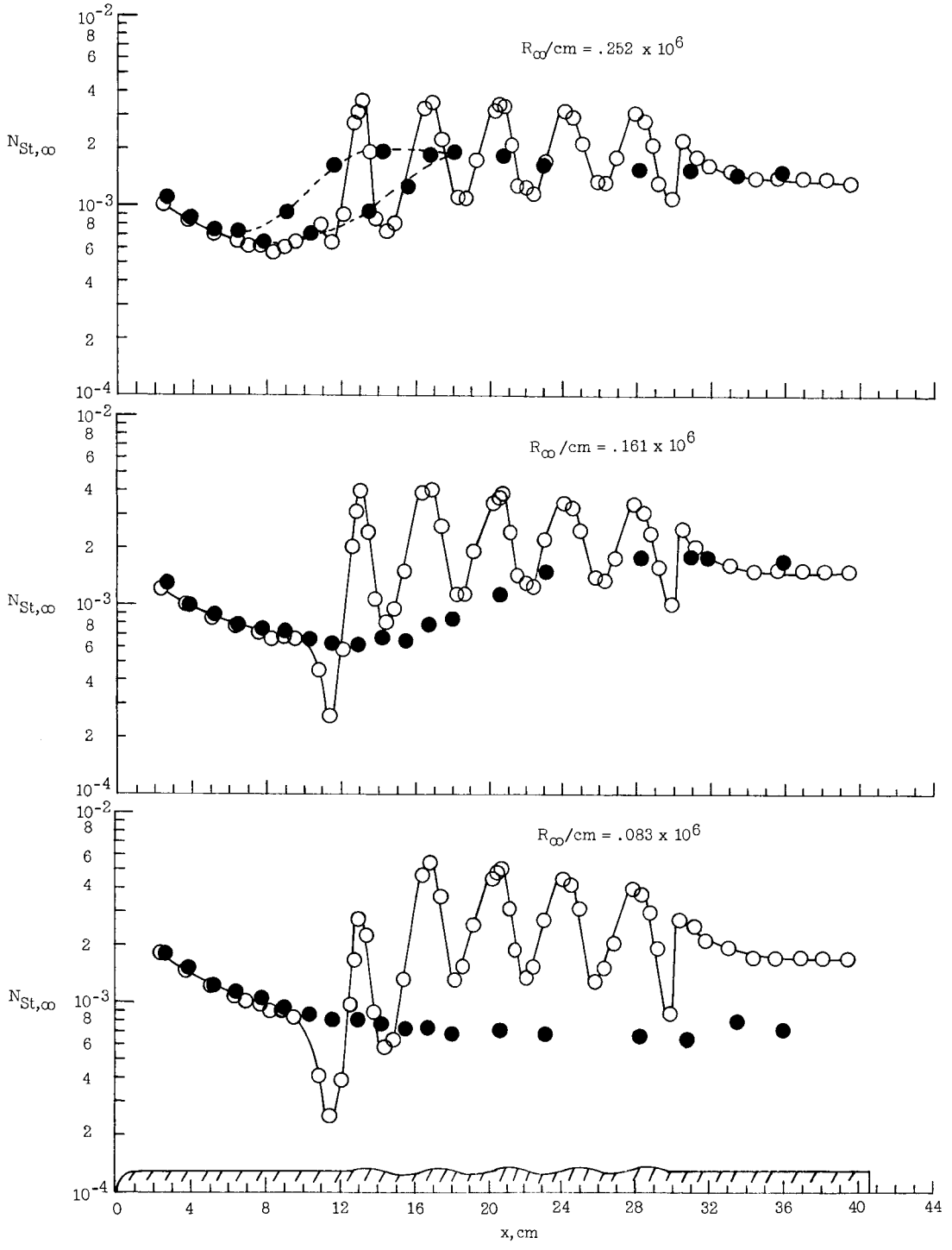

(e) $\alpha = 15^0$.

Figure 11.- Concluded.

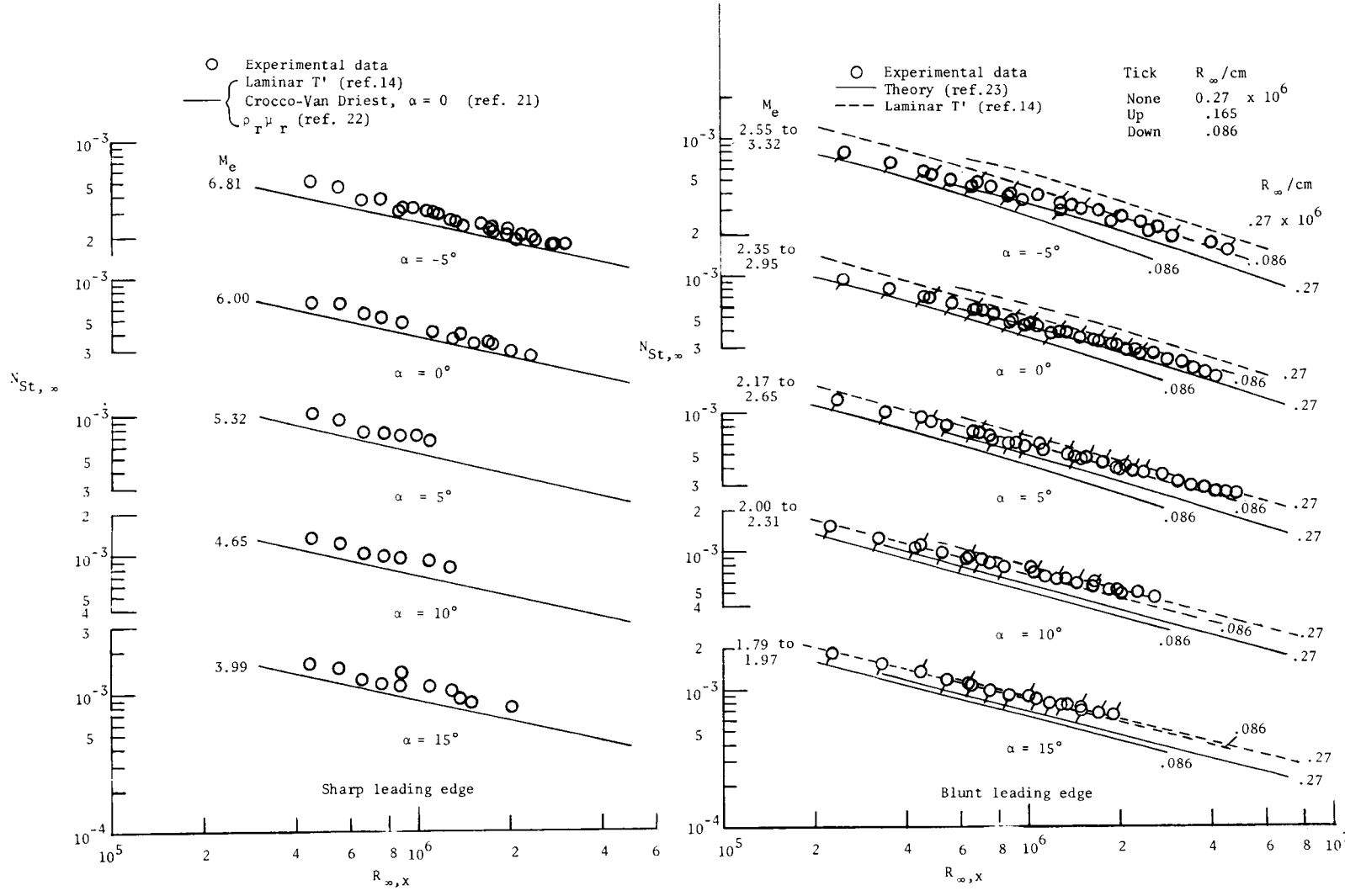

Figure 12.- Flat-plate laminar heating. $M_\infty = 6$; $R_\infty/cm = 0.27 \times 10^6, 0.165 \times 10^6, 0.087 \times 10^6$.

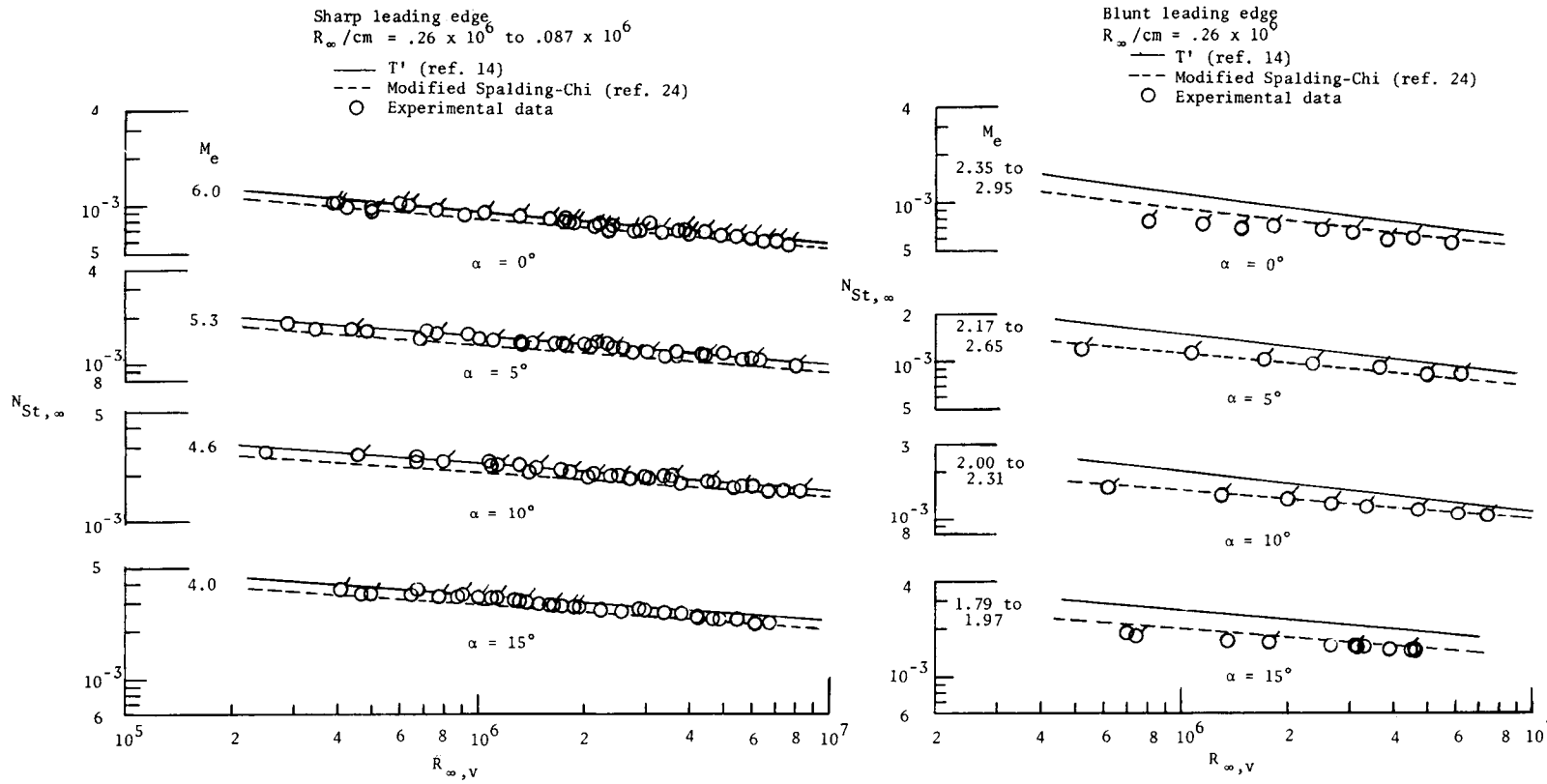

Figure 13.- Flat-plate turbulent heating. M_∞ = 6. Data with ticks indicate use of boundary-layer trip.

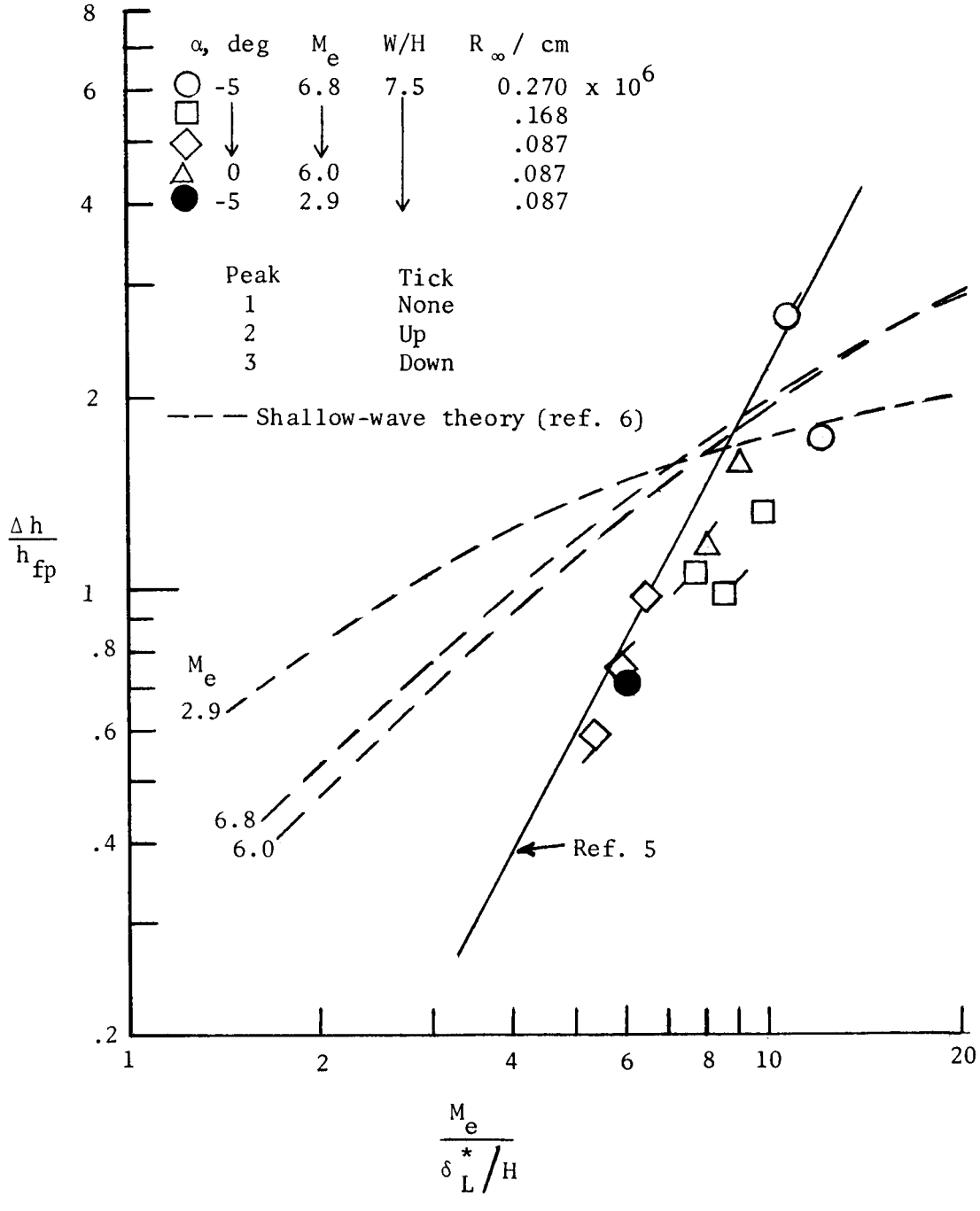

Figure 14.- Correlation of laminar maximum heating on multiple two-dimensional protuberances. $M_\infty = 6$; $T_w/T_t = 0.6$.

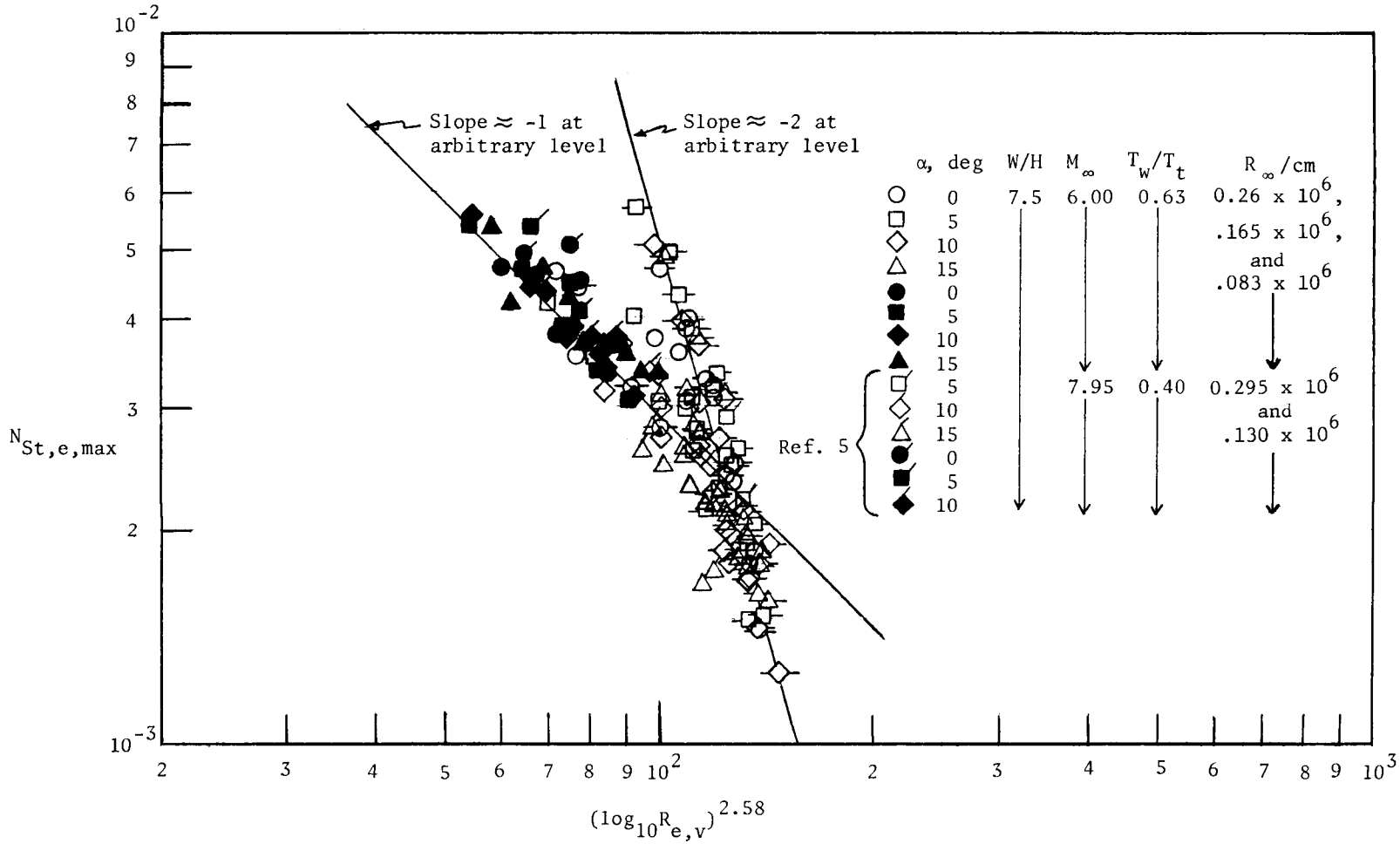

Figure 15.- Maximum turbulent heating for multiple-wave plates. Open symbols, sharp leading edge; solid symbols, blunt leading edge. Tick mark on each side of symbol indicates roughness data. (Data included for all waves.)

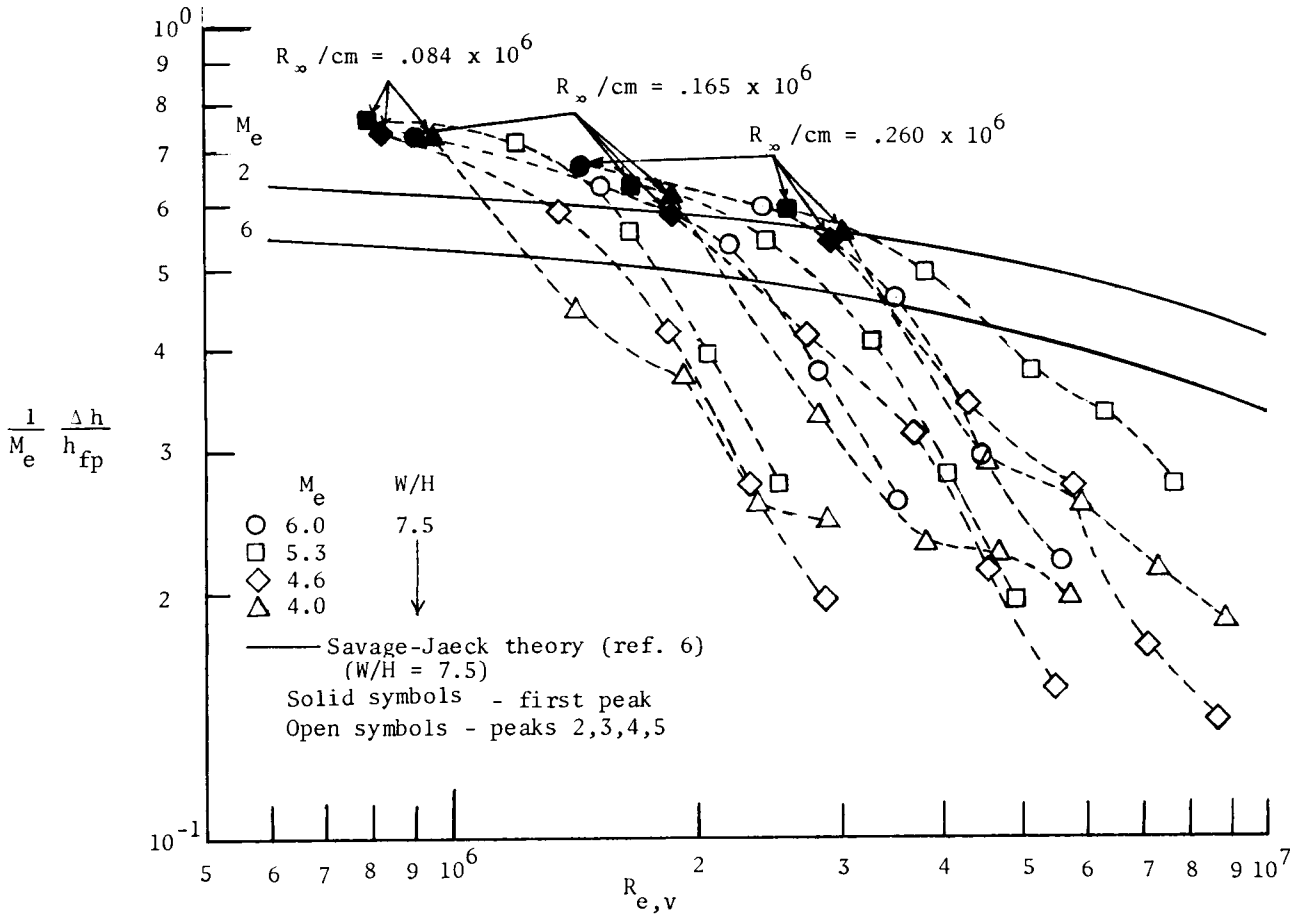

Figure 16.- Effect of local Reynolds number on turbulent peak heating for the sharp-leading-edge multiple-wave plate with roughness.

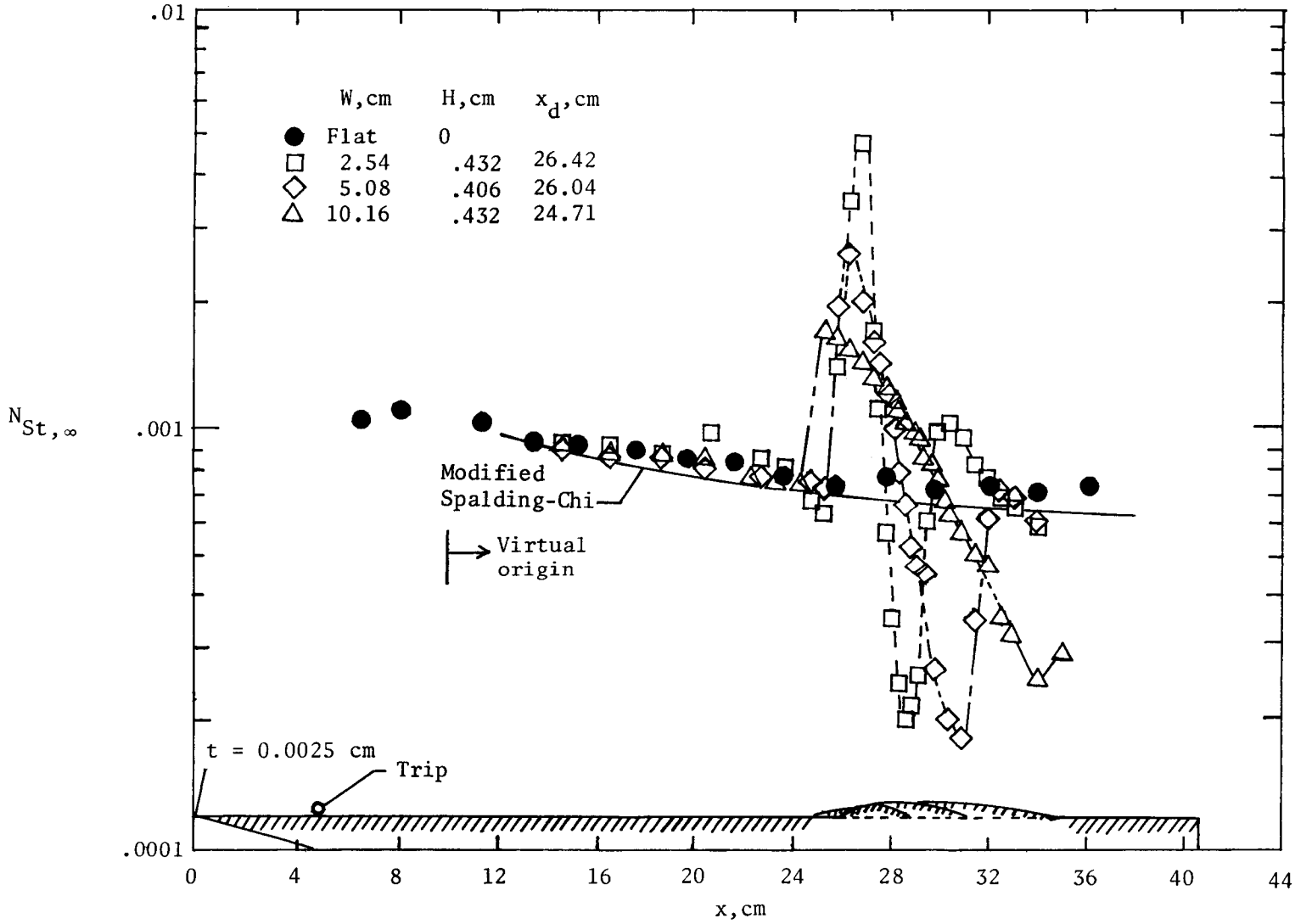

Figure 17.- Turbulent surface heating for a sharp flat plate with single two-dimensional sinusoidal surface protuberances. $M_\infty = 6$; $R_\infty/cm = 0.138 \times 10^6$; $\alpha = 0^0$.

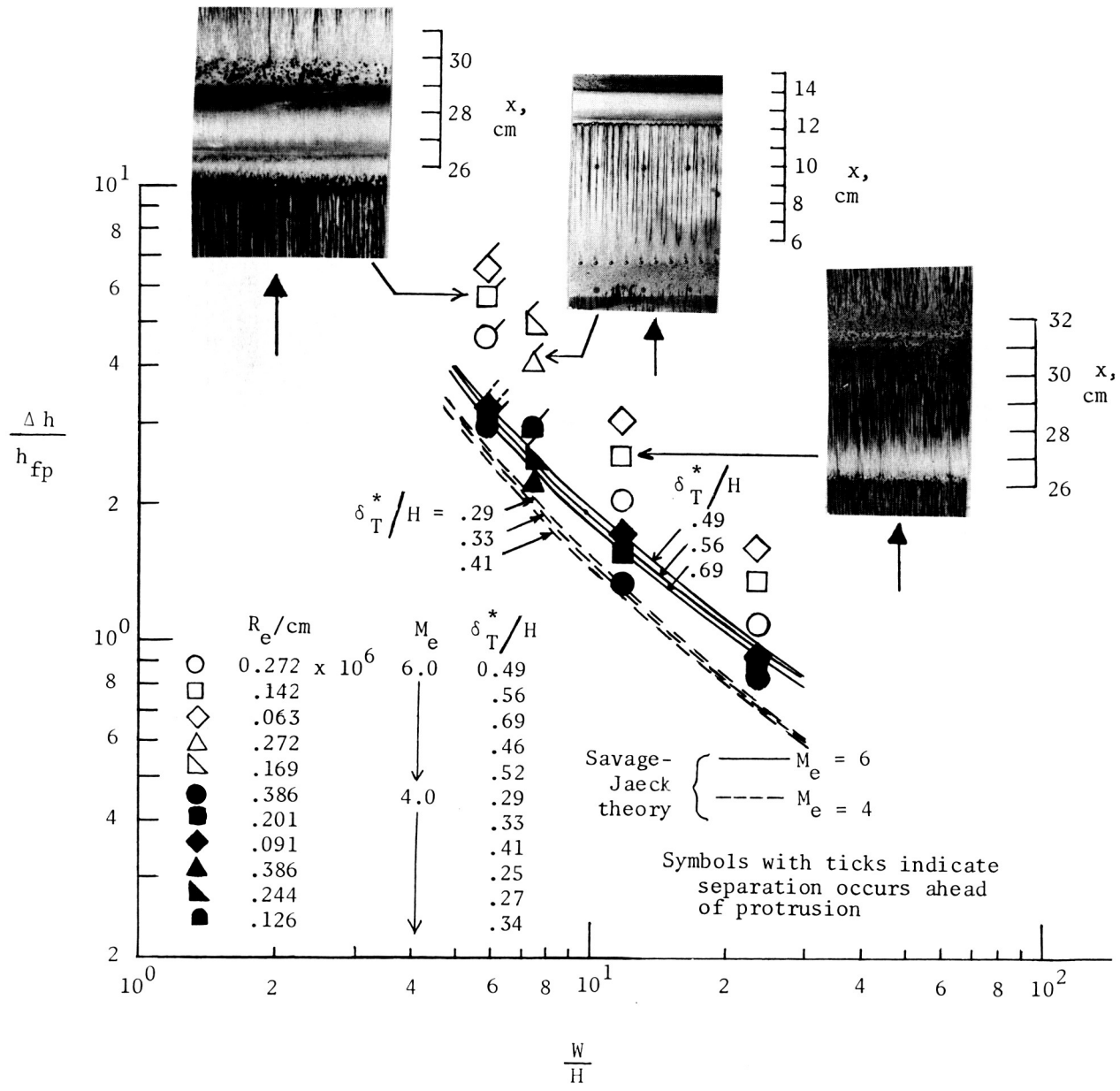

L-67-8721

Figure 18.- Effect of width-height ratio on turbulent peak heating for sinusoidal surface protuberances. M_∞ = 6. Boundary-layer trip 5.08 cm from the sharp leading edge.